THESIS
2
2000

MICHIGAN STATE UNIVERSITY LIBRARIES
3 1293 02106 1811

LIBRARY
Michigan State
University

This is to certify that the

thesis entitled

The Design, Construction, and Preliminary Testing of a Dynamic Fire Testing Facility

presented by

Andrew McIntosh

has been accepted towards fulfillment
of the requirements for

MS degree in Mechanical Engineering

Major professor

Date 1 May, 2000

O-7639

MSU is an Affirmative Action/Equal Opportunity Institution

PLACE IN RETURN BOX to remove this checkout from your record.
TO AVOID FINES return on or before date due.
MAY BE RECALLED with earlier due date if requested.

DATE DUE	DATE DUE	DATE DUE
DEC 2078 2003		

11/00 c:/CIRC/DateDue.p65-p.14

THE DESIGN, CONSTRUCTION AND PRELIMINARY TESTING OF A DYNAMIC FIRE TESTING FACILITY

By

Andrew W. McIntosh

A THESIS

Submitted to
Michigan State University
in partial fulfillment of the requirements
for the degree of

MASTERS OF SCIENCE

Department of Mechanical Engineering

2000

ABSTRACT

THE DESIGN, CONSTRUCTION, AND PRELIMINARY TESTING OF A DYNAMIC FIRE TESTING FACILITY

By

Andrew W. McIntosh

With the growing concern over the fire safety of new materials utilized in commercial and industrial applications, the need to quantify and properly characterize ignition and flame spread over potentially flammable surfaces becomes increasingly necessary. Effective tests of a material's flammability characteristics will both simulate actual combustion situations and allow for the isolation and measurement of the governing physical phenomena. The MSU Fire Tunnel is an experimental apparatus designed to test piloted ignition and flame spread over solid fuels subject to an external radiant flux and a forced parallel oxidizer flow. Special attention was given to establishing a well-controlled flow field in and around the fuel sample boundary layer. This, in addition to the use of a wider test section, can alleviate tunnel effects and flow-induced flame front inconsistencies. Tests of the various components in the MSU Fire Tunnel were completed in addition to preliminary flame spread experiments. The experiments indicate that the device produces a predictable, repeatable environment for flame spread testing.

For Gavin, Madeline, and
Bonnie

ACKNOWLEDGEMENTS

I would like to thank Dr. Indrek S. Wichman, my advisor, for his dedicated help and guidance. I would also like to thank Dr. John Foss for his input into the design problem. I would also like to acknowledge Dr. John McGrath for generously allowing me to use many of his laboratory resources.

I must acknowledge Scott Morris, who's expert advice helped me tremendously. I must also thank Mike McLean, who educated and encouraged me. I also must acknowledge Alptekin Aksan, whose tireless generosity, encouragement, and keen insights helped make this project possible. I would also like to thank Paul Hoke, who provided me with a great deal of invaluable advice and expert counsel in both the scientific and philosophical arenas.

I would like to thank my parents and grandparents who helped me, encouraged me and imparted me with a strong work ethic.

I would especially like to thank my wife, Bonnie, because without her patience and encouragement none of this would be possible.

TABLE OF CONTENTS

LIST OF TABLES

LIST OF FIGURES

NOMENCLATURE

A	area
a	minor axis length of the ellipse
b	major axis length of the ellipse
b	intercept of least-squares fit
C_q	effective linear cross-section of the combustion chamber
H	combustion chamber height
h	distance between plates
L	sample length
L_x	distance from the leading edge of the airfoil to the sample leading edge
m	slope
$\dot{m}''_{fuel,evap}$	rate of fuel evaporation
n	sample size
$\dot{q}''_{flame}$	heat flux from the flame to the sample surface
$\dot{q}''_{ext}$	heat flux from the radiant panel
Re_θ	Reynolds number based on momentum thickness
S_b	error in estimating the intercept
S_m	error in estimating the slope
S_y	standard error
T	temperature

U_∞	free stream velocity
W	ratio of the plate width to the distance between plates
w	plate width
X	plate length variable
X_m	normalized distance from contraction inlet
$\bar{x}$	sample mean

Greek Symbols

Δt_l	interval between successive flashes
Δx	quenching distance
Δx_f	thickness of flame
δ	boundary layer thickness
δ^*	displacement thickness
ϵ	emissivity
μ	true mean
ν	kinematic viscosity
θ	momentum thickness
σ	standard deviation
ξ	non-dimensionalized plate length variable
Ψ	heat flux loss to the surroundings
Ω	Ohms

INTRODUCTION

Background

A fundamental understanding of the mechanisms by which flames ignite and spread over materials is important in the design of materials for use in potentially hazardous environments. The chemical and physical properties of a potentially flammable material, the presence of background radiation or forced oxidizer flow, and the geometry of the material can all contribute to an increased risk of fire. Given the growing concern over the fire safety of new materials utilized in areas ranging from the automotive industry, to the housing market, to applications in aerospace engineering, the need to properly characterize the nature of ignition and flame spread over potentially flammable surfaces has become increasingly necessary. Furthermore it is necessary that this characterization be as systematic and scientifically based as possible.

Thermal radiation generated by surrounding flames influences ignition and flame spread over materials. Preheating by this "background" thermal radiation provides enough initial energy to sustain an exothermic reaction and is generally a prerequisite for flame spread over many flammable materials. A quantification of the preheating effect on material flammability is therefore of great importance in the field of fire safety.

One physical quantity that affects the ability of a fire to spread is its access to oxidizer. Ventilation-driven flows within a room, for example, often contribute to

flame spread. The nature of the resulting air flow and its interaction with the surface of a material determine the amount of convective heat transfer, which affects onset of ignition and the rate and direction of flame spread over the surface.

Buoyancy forces within the surrounding fluid affect fire behavior. The effect of buoyancy on the stability of a flame can be demonstrated using a match. If a match is lit and is held tip up, the flame travels downward (in the opposite direction from buoyancy-induced flow) at a predictable rate. This is known as wind-opposed flame spread. When the tip is held downward and the flame is allowed to travel in the same direction as the buoyancy-induced flow, stability breaks down and predictability of the spread rate decreases. This wind-aided flame spread usually occurs at a rate that is an order of magnitude higher than that of wind-opposed flame spread [1]. Additionally, wind-aided flame spread is characteristically unstable because acceleration is usually one of its inherent features [1].

Effective tests of a material's flammability characteristics will both simulate "real world" combustion situations and allow for the isolation and measurement of the governing physical phenomena. While no device in existence is capable of simulating and measuring all of the phenomena relevant to combustion, several devices (like the cone calorimeter and the Lateral Ignition and Flammability Test (LIFT)) have become standards for classifying simple combustion parameters. As the need to better classify some of the more subtle combustion characteristics of materials has increased, so has the required accuracy and fidelity of the

corresponding tests. In the following, various devices used to test flammability characteristics of materials are presented and discussed.

Existing Testing Devices

The Steiner tunnel test is a relatively large-scale, wind-aided test method used to determine surface burning characteristics of building materials [2]. A horizontally oriented sample is exposed to an ignition source at the bottom of one end and the fire is observed as it travels along the length of the material. Limited in its versatility, this crude, comparative test apparatus is one of the oldest flame-spread devices in existence. The fact that the results are normalized to an arbitrary standard reduces the usefulness of this device in the context of generalized engineering calculations.

The Cone Calorimeter consists of a cone-shaped array of radiant coil heaters imposing a known radiant flux upon a small sample placed near a pilot flame [3,4]. The Cone Calorimeter is capable of measuring the Heat Release Rate (HRR) of various materials indirectly by monitoring the oxygen consumption of the flame. The Cone Calorimeter, while effective for quantifying a few narrow parameters, is limited by its simplicity and is capable of measuring only "static" material combustion. The configuration of the device does not allow for quantification and isolation of various phenomena such as the effect of buoyancy-induced flows and the discontinuities in a flame front.

The flooring radiant panel tester apparatus (ASTM E 648) quantifies the level of radiant flux that a sample is exposed to [5]. This test device is capable of

determining a parameter described as the critical radiant flux for a solid fuel. While ASTM E 648 does allow an accurate variation and quantification of the level of radiant flux, the test geometry prevents variation of other environmental parameters.

The Lateral Ignition and Flammability Test (LIFT) devised by J. Quintiere [6] allows for the measurement of dynamic ignition and flame spread. This device consists of a radiant panel mounted opposite a fuel sample configured to allow flame spread over the sample surface. The flame within the LIFT draws its oxidizer from the ambient air (i.e., it is open to the surrounding quiescent atmosphere) and therefore makes it difficult to quantify the effect of oxidizer flow (buoyant, in this case) and oxygen concentration on the flame spread.

The Forced-flow Ignition and flame-Spread Test (FIST) devised by A.C. Fernandez-Pello allows an additional level of sophistication [7]. FIST consists of a combustion wind tunnel directing flow into a test chamber. Within the test chamber a sample is vertically mounted opposite a radiant panel. This device allows quantification of flame spread and ignition phenomena subject to both forced flow and radiant flux. The small scale of the device and its conditioning of the fluid flow within the test chamber limit its effectiveness for various sorts of tests although the overall success of this approach has been noteworthy.

The MSU Fire Tunnel

The device presented in this study, referred to herein as the MSU Fire Tunnel, is a modification of the FIST. Because the MSU Fire Tunnel enables a

wider sample to be tested, discontinuities through the flame front can be observed. The effect of forced (oxidizer) flow on ignition and flame spread over the sample surface was examined. Additionally, because the forced oxidizer flow was carefully conditioned in the combustion chamber a sample's onset to burn and subsequent combustion can be modeled with greater ease.

The goal of this study was to design, build, and test a device that recreates the conditions under which ignition and flame spread occurs over vertically oriented materials in order to quantify various material flammability characteristics. Because background (thermal) radiation can so strongly influence the growth and spread of a fire, its effect was simulated and carefully examined in the experimental device.

A secondary goal was to enable the device to be adapted for future experimental work. For this reason the combustion wind tunnel and the supporting peripheral equipment were designed in a modular fashion. This feature provides experimental flexibility because each component can be modified and combined with other components. For example, combustion experiments examining the influence of simulated micro-gravity environments on flame spread are currently being designed to connect directly with components in this device.

CHAPTER 1

LITERATURE REVIEW

1.1 Introduction

Flame spread over solid materials is a complex phenomenon that does not easily lend itself to quantitative analysis. As a result, flammability characteristics of materials have often been determined empirically. Even for the empirical tests, a need exists to relate the empirical measurements and results to a systematic theory in order that the results can be properly interpreted and used in engineering estimates. Although analytical and numerical models have been used to simulate parameters such as flame spread rate, heat release rate (HRR), and char formation rate, experimentation remains the most reliable and accurate method for determining material flammability parameters.

Flame spread and flammability standards for the burning of solid fuels have been developed using many test methods. Among these test devices are the Steiner tunnel test (ASTM E 84 –97a), the cone calorimeter (ASTM E 1740 – 95), the flooring radiant panel tester apparatus (ASTM E 648 –97), and the Lateral Ignition and Flammability Test (LIFT) (ASTM E 1321 – 97a). These test devices are capable of measuring flame-spread rates and possibly other flammability parameters of materials. While it is well accepted that each of these test methods yields repeatable results, they are limited to providing data that cannot be adequately generalized and compared to analytical models which include the influences of fluid flow and mass transport [8]. This limitation is primarily due to the nature of the experimental designs, their respective

treatments of the oxidizer flow in the test apparatuses, and the relation (or lack thereof) to established engineering theoretical correlations.

1.2 The Steiner Tunnel Test

The Steiner tunnel test is a relatively large-scale, wind-aided test method used to determine surface burning characteristics of building materials. In this test method the material to be tested is oriented horizontally and exposed from below to an ignition source. The tunnel has a 0.14 m^2 cross-section and is 7.6 m long. This type of test device was first developed at Underwriters Laboratories around 1922 for the purpose of determining the effectiveness of then current "fire-proofing" paints that were being promoted at the time [2]. As the need to obtain more accurate results increased, the test apparatus design was refined to correct for variations reported in flame spread measurements.

Test methods of the Steiner tunnel type generate two indices: the flame spread index (FSI) and the smoke density index (SDI) both of which classify a material's flammability behavior relative to a standard. The FSI is a parameter generated by measuring the area under the distance versus time curve (ignoring any flame recession) for a test material and comparing that to a section of red oak flooring [2]. The SDI is obtained, similarly, by comparing the smoke density time curve (measured using light absorption techniques) produced by red oak to that of the test specimen.

The Steiner tunnel test has many limitations that restrict its usage and the applicability of the test results. While useful in generating rough comparative

data for some materials, it is not capable of producing results that can be compared to externally developed engineering formulas. Additionally, this test is capable of producing realistic results only for materials that maintain their structural integrity when fully heated, thus eliminating many polymers as candidates for testing and evaluation.

Problems also exist with the calibration technique. Calibration of this test device involves altering a variety of conditions in the test chamber until a prescribed FSI for red oak is obtained. Because there are many possible combinations of operating conditions that could produce this FSI, a variation between "calibrated" devices may occur.

When polymeric samples are tested in the Steiner tunnel a mesh support must be used to keep the sample from sagging while the test is running. This mesh support can act as a heat sink thus producing artificially low FSI data. A polymeric sample that tends to delaminate during the test will produce falsely high FSI data. This lack of versatility becomes more important as polymeric materials are increasingly used in commercial and industrial applications.

Because of the relative nature of the data generated by the Steiner test, it is incapable of producing data in a form that can be used in engineering calculations, thus the data generated cannot be compared to analytical generalizations of material flame spread characteristics. While the Steiner test has many desirable features, it is unsuited, for many reasons, to the systematic study of flame spread over materials.

1

s

b

p

in

va

a

d

(l

d

sa

fl

a

m

fl

co

co

re

co

sa

1.3 The Cone Calorimeter

The Cone Calorimeter is a test apparatus primarily used to determine simple material flammability parameters, including heat release rate (HRR) of a burning sample, sample mass loss rates, time to sustained flaming, and smoke production [3,4]. According to [3,4], the rate of heat release is one of the most important variables in determining the hazard from a fire. The importance of this variable along with the relative accuracy with which it can be measured using this apparatus make the cone calorimeter one of the most important devices for determining a material's fire hazard. Because this test apparatus is now ISO (International Standards Organization) approved, it is used in nearly all developed countries including the USA, Canada, Western Europe, and Japan.

The test apparatus consists of an enclosed bench upon which a solid fuel sample is mounted horizontally. The sample is exposed to a prescribed radiant flux (between 0 and 100 kW/m^2) until ignition occurs. Experiments may include an outside ignition source (such as a spark or a pre-mixed flame) or the sample may simply auto-ignite. This requires the formation (by sample gasification) of a flammable mixture in the air (or other oxidizer) above the sample. During combustion, exhaust gasses are collected in an overhead hood where oxygen concentration and flow rate are measured to determine the sample's HRR.

This test relies on the notion that, in most cases, there is a direct relationship between the net heat of combustion and the oxygen required for combustion [3,4]. In order to correlate the measured oxygen concentration with sample HRR the sample total burning area must be recorded over time. The

HRR is cumbersome to compute because uneven flame fronts and the occurrence of flame regression make accurate measurement of the total burning area, at any one time, difficult.

The cone calorimeter is not designed to measure flame-spread rates but the calculation of the spread rate may be performed in an appropriate way with the data taken from a typical test. For this reason the cone calorimeter has been used to estimate rates of flame spread over materials. But just as with the Steiner Tunnel, the air entering the cone calorimeter test chamber is ordinarily not well regulated. The airflow near the burning surface is dominated by natural convection and is therefore generally unpredictable. The dominance of buoyancy induced flow complicates the physics of the fuel/oxidizer interaction to the degree to which it prohibits accurate mathematical modeling.

1.4 Flooring Radiant Panel Tester Apparatus

According to [9], the ASTM E 648 (flooring radiant panel tester apparatus) is one of the few test devices that actually give results in usable engineering terms. This test device is capable of determining a parameter described as the critical radiant flux for a solid fuel. The critical radiant flux is defined in [5] as the level of incident radiant heat energy on the floor covering system at the most distant flame-out point. It is reported in W/cm^2. This test device relies on the assumption that the critical radiant flux is an indicator of the flame-spread rate and therefore the flammability of a material.

The flooring radiant panel tester apparatus consists of a radiant panel mounted at an angle of 30° from the horizontal directly above the solid fuel sample in order to deliver a non-uniform heat flux distribution over the sample surface. The sample is ignited using a pilot burner at the end closest to the radiant panel, where the radiant intensity is the highest. The maximum distance that the flame travels over the surface is recorded and matched to the measured radiant flux at that point. This is considered to be the lowest level of radiant flux that will still support sustained burning.

Radiant flux is considered to be one of the parameters that most closely governs the behavior of flame spread over flooring materials because buoyancy tends to convect heat away from surfaces to which flames may travel [5]. In contrast, the radiant flux is a constant source of thermal energy to the surface. However, the critical radiant flux obtained from this test offers little insight into the nature of flame spread subject to radiation at levels higher than the minimum required for sustained burning. This is troubling given that most flame spread in actual fires will occur under higher levels of radiant flux than the critical level for sustained burning. Additionally, the flooring radiant panel tester apparatus is subject to the same problems that hinder the Steiner tunnel and the cone calorimeter, namely the dominance of buoyancy induced oxidizer flow near the sample surface.

1.5 The LIFT

The LIFT (ASTM E 1321-97a) devised by J. Quintiere, is a test apparatus designed to determine many material flammability parameters. These include the minimum surface heat flux necessary for sustained burning, the temperature necessary for ignition, an effective material thermal inertia value, and a flame heating parameter pertinent to lateral flame spread [6]. These parameters can be used to obtain the time to ignition and the lateral flame spread velocity over various combustible materials.

The test apparatus consists of a vertically mounted solid fuel sample positioned directly opposite a radiant panel angled 15° from the plane of the sample. The radiant panel is designed to deliver a varying heat flux over the sample's surface. Two separate tests are conducted during a trial run. The first test measures ignition of a sample, the second measures the flame spread rate over the sample surface. The ignition test is designed to determine the time required for the sample to ignite by an acetylene-air pilot flame. The flame spread test exposes the sample to a given radiant flux using the acetylene-air flame as a pilot. Data are recorded as the flame front moves laterally across the sample surface.

The LIFT is capable of producing data that are closer in nature to the parameters used to describe other, simpler phenomena. The results are not produced relative to an arbitrarily chosen standard as with the Steiner tunnel, for

example. Analogously to the description of material insulative properties using dielectric strength, the LIFT is capable of producing results that can be generalized for other, similar materials under different conditions using the resulting theoretical correlations. Even though the LIFT does make it possible to present results in engineering terms it is likely that the measurements are not as universal as initially expected, especially for forced flow conditions. This occurs because the air (or oxidizer) flow across the sample surface in the LIFT is uncontrolled buoyant flow produced by combustion. The uncontrolled flow can introduce large testing variations. Fernandez-Pello et. al. have shown, using the FIST device, that critical radiant flux for ignition and ignition temperature are not inherent material characteristics but dependant on environmental (and other) factors [7]. The dependence of the critical radiant flux and the ignition temperature on factors that were not controlled in the LIFT apparatus further emphasizes the need to control, condition, and monitor the incoming oxidizer flow.

1.6 The FIST

The Forced-flow Ignition and flame-Spread Test (FIST), developed by A.C. Fernandez-Pello et al., is a test apparatus that is similar to the LIFT except that the oxidizer flow is forced into the combustion chamber. Buoyant convection over the burning surface is replaced by forced convection. The FIST was designed to determine ignition temperatures, flame spread rates, as well as other pertinent flammability parameters of solid fuel samples subjected to an external

radiant flux under parallel forced oxidizer flow conditions. While the test apparatus is still in the developmental stages it is producing some interesting preliminary results.

The FIST consists of a small-scale combustion wind tunnel that forces flow into an enclosed test section [7]. The test section contains a vertically oriented sample mounted directly opposite a radiant panel. The radiant panel is mounted on tracks allowing it to be heated to a constant temperature and then slid into place so that the sample surface is impulsively heated from the time the test commences. In other words, this feature eliminates a power-up phase of radiant sample heating (which was present in the LIFT). The sample is ignited at its top edge using an extremely hot nickel-chromium wire and thereafter flame spreads downward over the sample surface.

Just as with the LIFT, the FIST performs two separate tests. One is an ignition test and the other is a flame-spread test. The ignition test is conducted for a given set of flow conditions and a given radiant flux. The radiant panel is slid into place and the time to piloted ignition is recorded. The flame-spread test begins when ignition occurs near the top of the sample. The rate at which the flames spread over the sample surface is recorded. These data are recorded for a variety of flow and environmental conditions.

The FIST, though not yet sanctioned for use by any standards committee (e.g. ISO, ASTM, ect.), takes a significant step toward isolating and allowing for the independent control of the various phenomena that are present in solid fuel flame spread. However, given the importance of the near-surface fluid dynamics

it is not altogether clear that further work wouldn't improve the design of the FIST. According to J.L. Cordova, J. Ceamanos, and A.C. Fernandez-Pello the major effect on the ignition time (of a solid fuel) appears to be due to convective transfer variations at the fuel surface [10]. It is also true that the convective flow has a very large influence on the flame-spread process, thus demonstrating that convection influences both FIST tests, the ignition and spread tests. Because of this strong dependence that material flammability characteristics have on the nature of the oxidizer flow, careful treatment of the oxidizer flow in the tunnel is required.

Effective flame spread test methods will both simulate realistic fire conditions and allow for the isolation and measurement of several critical environmental parameters. While several of the test apparatuses examined are effective in comparing relative flammability characteristics, few possess the capability to produce even some of their results in engineering terms.

CHAPTER 2

THE EXPERIMENTAL DEVICE

2.1 Introduction

The MSU Fire Tunnel is an experimental device designed to determine both ignition and flame-spread characteristics of solid fuels subject to both an external radiant flux and a forced oxidizer flow.

The MSU Fire Tunnel consists of four main components: the settling chamber, the conditioner, the converging duct, and the combustion chamber (Fig. 2.1). Below is a brief outline of each component's role in the device followed by a more detailed description.

The first of the four main components is the settling chamber. Air is injected into this chamber with a blower. A calibrated elbow meter measures the volume flow rate of the injected air. The pressurized settling chamber acts as a plenum, allowing the injected air to become nearly quiescent.

Next, the air proceeds through the flow conditioner, which consists of a series of wire cloth screens and a honeycomb section positioned perpendicular to the bulk flow direction. The conditioner section serves to dissipate any turbulent eddies that may remain in the flow.

The converging duct then directs the flow from the larger cross-sectional area of the conditioner into the smaller cross-sectional area of the combustion chamber. In addition it serves to make the flow more uniform, speed up the free

Blow

Fig

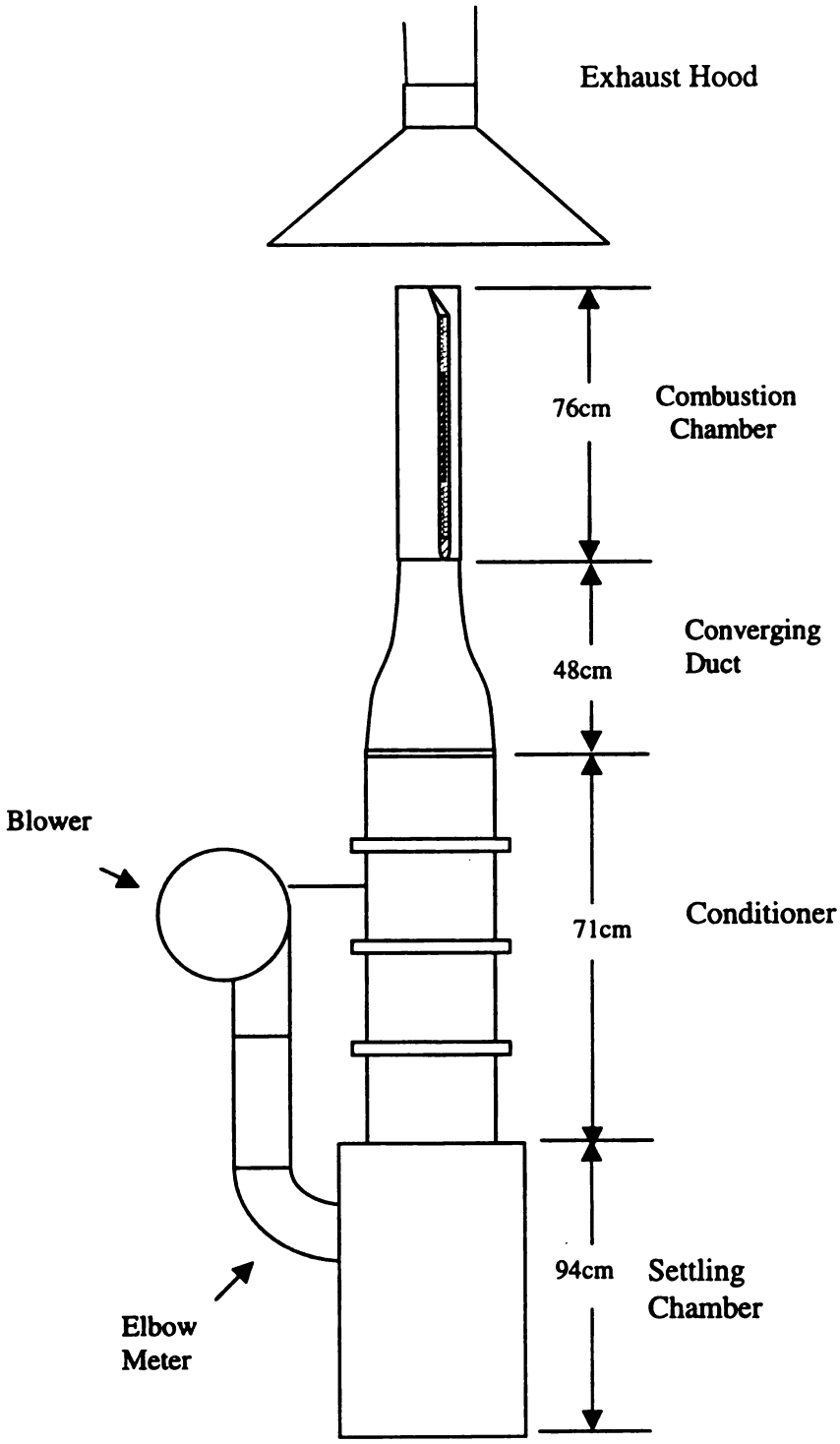

Figure 2.1 Major components of the MSU Fire Tunnel.

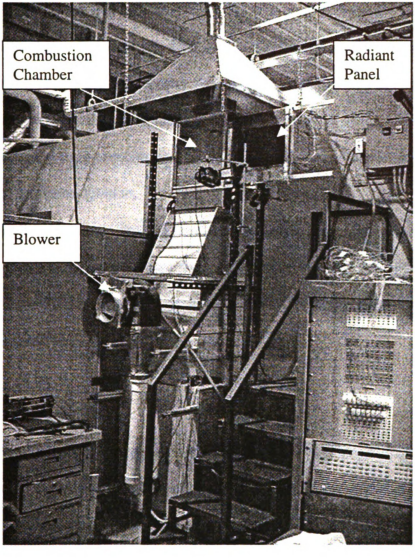

Figure 2.2 The MSU Fire Tunnel, note the radiant panel is slid out of the combustion chamber.

stream flow, reduce the turbulence intensity, and compress the boundary layer.

The fully conditioned and uniform airflow is then directed into the combustion chamber. Within the combustion chamber, a vertically oriented fuel sample is placed directly opposite a radiant panel. An extremely hot nickel-chromium wire (approximately 800 °C) positioned near the sample surface acts as a pilot for flame ignition.

As the sample is ignited, the flame front begins near the top of the sample and proceeds downward. After sample burning is complete, the flame is quickly extinguished with an injection of nitrogen gas, while the products of combustion are exhausted via a fume hood.

2.2 Settling Chamber

Wind tunnels are usually constructed such that flow is induced by creating a pressure lower than atmospheric in the downstream region and drawing from the quiescent surroundings. This technique, while effective at eliminating flow inconsistencies within the test chamber because air is drawn in with virtually no initial momentum, is inapplicable for most combustion wind tunnels. Hot products of combustion would do damage to any prime mover position close to the outlet of the test chamber.

Additionally, if careful regulation of the oxygen content (by injecting a known quantity of nitrogen or oxygen) within the combustion chamber is required, downstream induction makes it necessary to completely seal off the upstream

portion of the tunnel. If any leaks were to occur in the upstream portion of the tunnel they would change the net oxygen concentration of the oxidizer flow. Varying the oxygen concentration of the flow going into the combustion chamber by upstream injection of oxygen or nitrogen requires the a knowledge of the volume flow rate of nitrogen or oxygen and the volume flow rate of air.

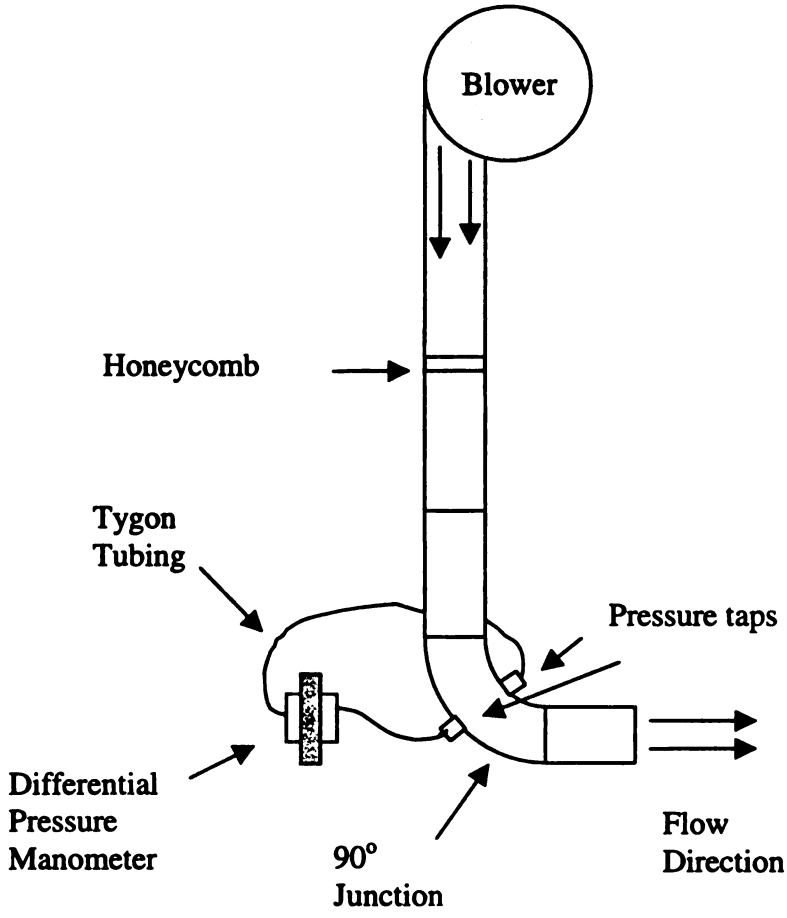

Figure 2.3 Blower and elbow meter (including the differential pressure manometer).

In order to know what the volume flow rate of air is (for the low volume flow rates examined in this study) the inlet cross-section must be constricted down to a rather small area, thus negating the advantage of downstream induction altogether.

Air is injected into the settling chamber using a Dayton ½ hp blower (Dayton PSC 4C831A). The flow rate is regulated with a sliding gate at the blower inlet. The blower is attached to 7.6cm diameter PVC pipe that directs flow into the settling chamber.

In order to measure the flow rate, an elbow meter was constructed. The pipe leading to the settling chamber is fitted with a 90° junction. Pressure taps were drilled into the inner and outer bends of the 90° junction.

Tygon tubing was extended from these pressure taps to a differential pressure manometer (MKS Baritron model #225AD-00010AABS, capable of measuring pressure differences from 0 to 1244 Pa, calibrated to in-H_2O). The Baritron pressure transducer is powered by a Power-One linear power supply (Power-One, HB28-1-A , 28 volts at 1 amp). The pressure transducer, 90° junction, pressure taps, etc. are collectively known as the elbow meter.

The elbow meter was calibrated using a correlation between the pressure difference displayed by the output of the manometer and the velocity in the combustion chamber. This correlation (Fig. 2.4) was developed over a range of velocities by adjusting the damper plate at the blower inlet. The fin (discussed in Chapter 3) was attached to the trailing edge of the sample holder).

Velocities were measured in the center of the combustion chamber using a TSI IFA 300 Constant Temperature Anemometer. A least squares linear regression analysis was performed. The equation for the linear curve fit is y= 0.9755x + 0.3446. The R^2 value is 0.99.

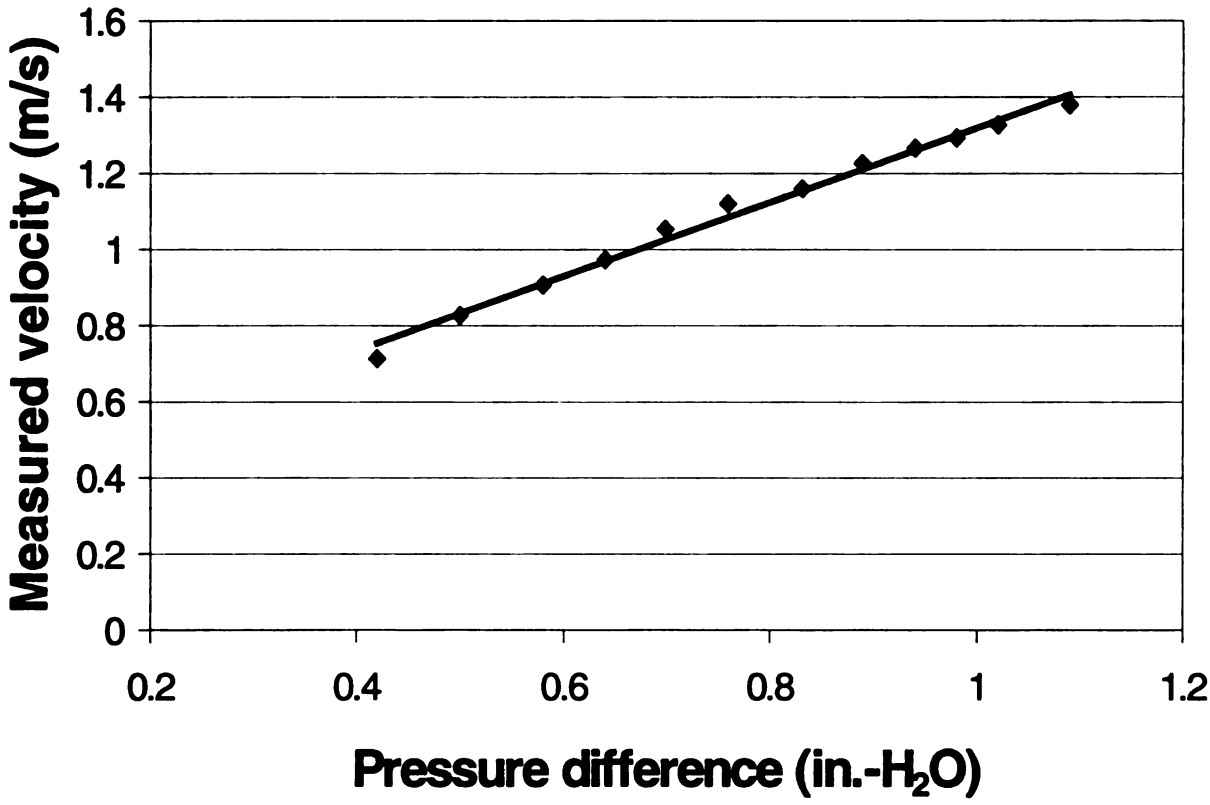

Figure 2.4 Calibration curve for the elbow meter.

Honeycomb was placed within the PVC pipe between the blower and the elbow meter. The 2.5cm thick honeycomb consists of a bundle of plastic tubes (similar to drinking straws) bound together. This suppresses any vorticity and inconsistencies in the airflow generated by the blower. As the air passes through the elbow meter it enters the sealed settling chamber where its velocity drops.

The settling chamber also serves as the structural base for the MSU Fire Tunnel. Four Unistrut beams extend from the settling chamber's plywood sides and run up the entire length of the MSU Fire Tunnel. These beams are bolted to a wood frame within the settling chamber. A steel platform beside the MSU Fire Tunnel allows for access to the combustion chamber (Fig. 2.2).

2.3 Converging Duct and Conditioner

As the oxidizer flow emerges from the settling chamber it passes through a series of conditioning structures. Honeycomb and screens (wire cloth) are positioned inside the conditioner duct orthogonal to the mean flow direction. This is intended to suppress vorticity and turbulent eddies that may have formed within the settling chamber.

The cross-sectional area of the conditioner duct is different than that of the settling chamber, requiring the use of a lip at the inlet of the conditioner. Two-inch PVC pipe was cut in half and secured to the edge of the conditioner inlet, thus providing a smooth transition for the flow from the settling chamber to the conditioner.

In order to accelerate, direct, and decrease turbulence in the oxidizer flow a contraction was built. The geometry of this contraction was chosen based on the study of [11], which outlines the design of two-dimensional wind-tunnel contractions. A two dimensional contraction was chosen because it provided the required plane symmetric flow within the combustion chamber and was relatively easy to construct. A one-dimensional contraction was not used in this study because of the desire for a plane symmetric velocity profile within the combustion chamber. A three-dimensional contraction was not chosen due to the complexity of its construction and an axisymmetric velocity profile was not required within the combustion chamber.

The size of the two dimensional contraction was determined based on the dimensions of the combustion chamber. The outlet of the contraction has the same dimensions as the inlet of the combustion chamber. The contraction ratio (defined as the area of the contraction inlet divided by the area the contraction outlet) was chosen as five [12].

The mathematical method for determining the geometry of a contraction involves piecing together two cubic polynomials. The location at which these cubic polynomials meet (defined as X_m) is determined by the chosen contraction ratio, the virtual origin of the boundary layer, the maximum wall pressure, the separation point of a turbulent boundary layer, as well as other factors. The quantity X_m is a normalized distance from the contraction inlet representing the location where the cubic polynomials meet. X_m is defined as zero at the contraction inlet and unity at the outlet. Once the point at which the two cubic

polynomials met was chosen, a computer program was employed to generate the geometry [13]. This computer program generates a series of points that were then plotted in Excel. The points depicted in Figure 2.5 describe the geometry of the converging duct.

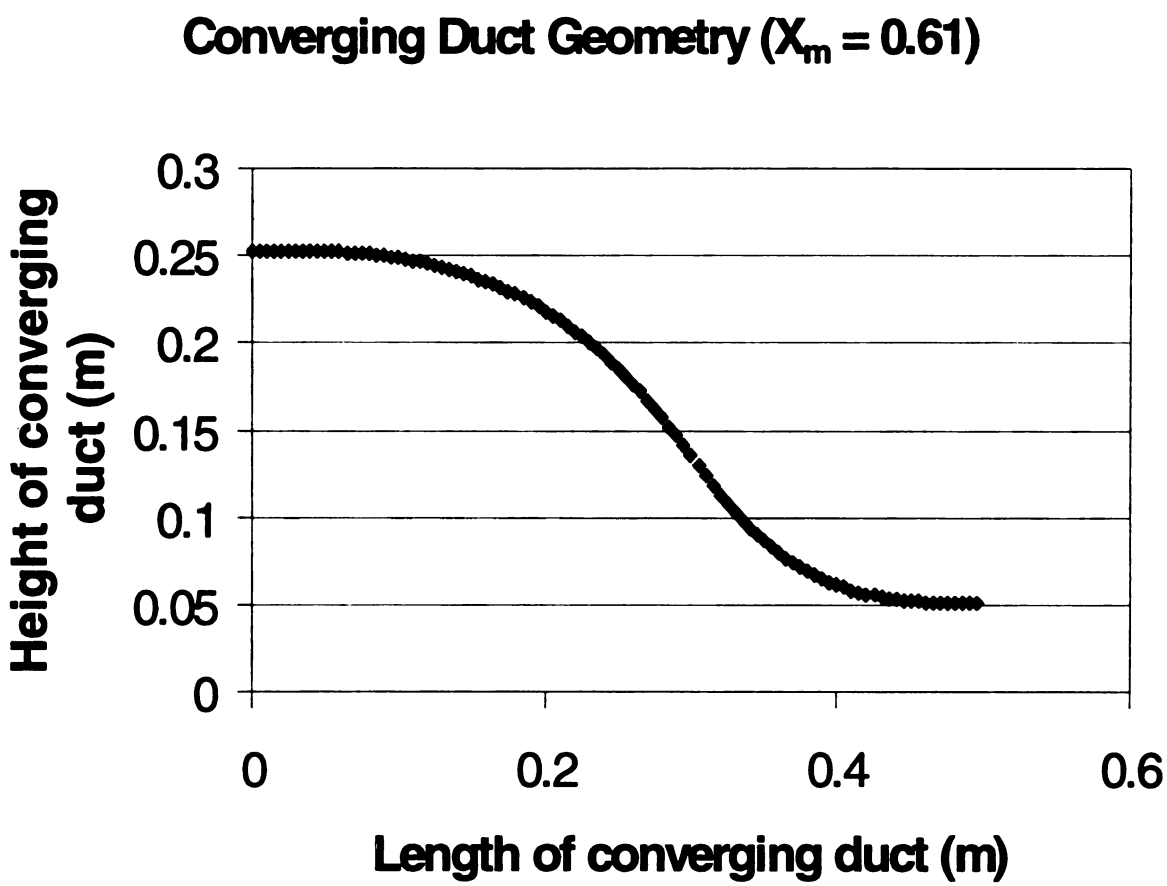

Figure 2.5 Converging duct geometry, X_m = 0.61.

The contraction was constructed using an aluminum frame and flexible plastic sheets. The desired contraction geometry was cut out of a piece of

1.6mm thick aluminum sheet metal using a computer-controlled mill that interpolated between the points provided to create a continuous cut. A frame was created from these aluminum shapes, and the plastic sheets were glued into place with an epoxy called Plastic Welder.

2.4 Combustion Chamber

The combustion chamber rests atop the contraction and is the location of the flame-spread tests. The aluminum frame of the combustion chamber is mounted to the Unistrut supports. A non-combustible Marinite board mounted within the combustion chamber acts as a sample holder. Strip heaters bolted to a sliding aluminum frame (collectively known as the radiant panel) can be heated up outside of the combustion chamber and then rapidly slid into place, thus providing the sample with a relatively time invariant impulsive heat flux. The wall behind the sample holder is a 1.6mm thick aluminum plate. The sides of the combustion chamber are 6.4mm thick Pyrex glass.

2.4.1 Sample Holder

The sample holder consists of an aluminum tray with a 90° bend at one end. A Marinite sheet with a thickness of 1.9cm was placed within the tray. The Marinite sheet had a 25.4cm x 22.8cm x 1.3cm square opening cut into its center using a router. The samples that were burned fit into this space.

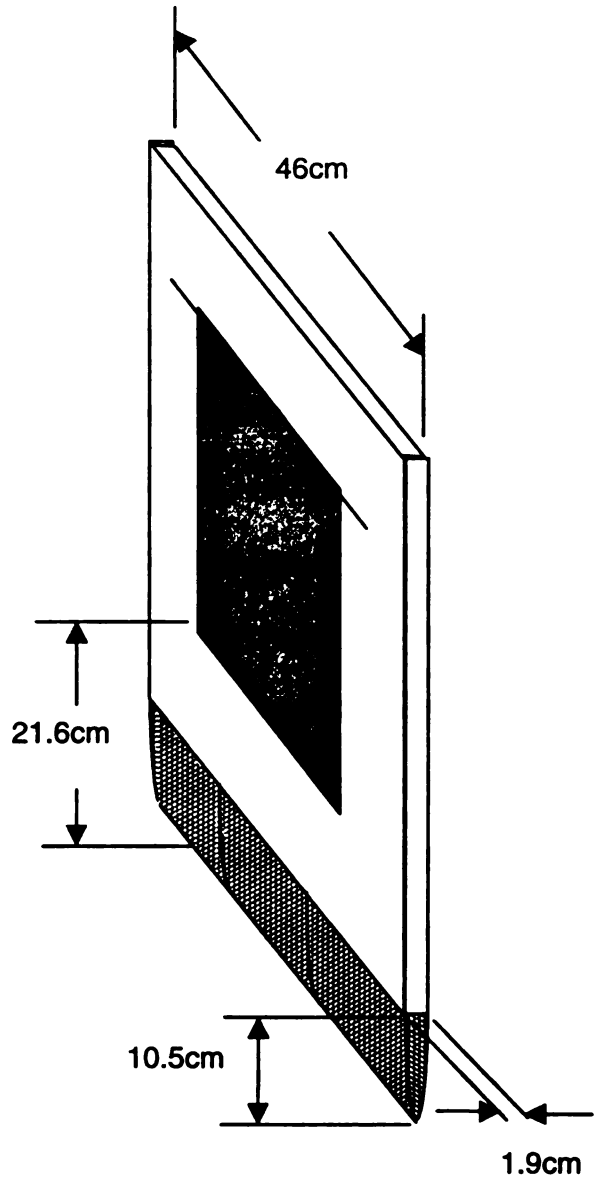

Figure 2.6 The sample holder of the MSU Fire Tunnel. The 10.5cm section is the airfoil leading edge, cut from aluminum using the EDM. The three sections are joined by a threaded rod. Shown also are the sample, 21.6cm downstream of the leading edge.

The sample holder was fitted with an airfoil (bolted to the 90° bend) that was designed to create a stagnation point at its leading edge. The airfoil has a cross-section that is half of a 10:1 ellipse. In terms of the fluid dynamics, this is the most important feature of the combustion chamber because it fixes the location of the boundary layer leading edge at the stagnation point on the ellipse [14]. The equation used (an equation for an ellipse) was $y=[b^2(1-x^2/a^2)]^{1/2}$, where a is the minor axis and b is the major axis of the ellipse. This equation was used in a program called Ez-Cam to generate a series of points for a computer controlled Electrical Discharge Machine (EDM). The EDM cut three 6" long, solid aluminum sections of the airfoil from three blocks of aluminum that were secured together using threaded rod. The airfoil was then bolted to the sample holder.

Dry wall filler was used to fill in the small gap between the trailing edge of the airfoil and the leading edge of the Marinite board. It was sanded to create a smooth transition for the oxidizer flow. A sample (1.3 cm thick) is secured onto the void in the Marinite sheet and the entire sample holder was placed into the combustion chamber.

The solid fuel samples used were 25.4cm x 22.8cm x 1.3cm clear Plexiglas G. This type of Plexiglas is cast, making it ideal for ignition and flame spread experiments because it does not melt or drip much. The fuel sample has mounting holes pre-drilled and is secured to the sample holder with nine steel mounting screws. These screws penetrate halfway into the fuel sample.

When the sample is placed into the sample holder, small gaps exist between the Marinite edge and the fuel sample edge. All the gaps except the one at the leading edge were filled with fiberglass insulation. The gap at the leading edge was filled with dry wall filler and sanded until smooth. This created a smooth transition for the flow from the sample holder to the fuel sample.

.

2.4.2 Ignition Assembly

Nickel-Chromium resistive heating wire was used to ignite the sample. The wire (Omega Engineering, Part # NI80-015-50ft) is 80% Nickel and 20% Chromium with a resistance of 8.435E-2 ohms/cm.

The heating wire was wrapped around a hollow ceramic rod with a 3mm diameter. Two steel wires insulated by hollow ceramic rods (6mm outer diameter, not shown in Fig. 2.7) carry current through the combustion chamber walls to the Nickel-Chromium wire and also act as structural support for the ignition assembly.

The ignition assembly was placed near the trailing edge of the sample, directly on the surface of the sample. A current of 5 amps raises this wire to a temperature of approximately 800° C. A variable voltage transformer was used to supply this current to the ignition wire.

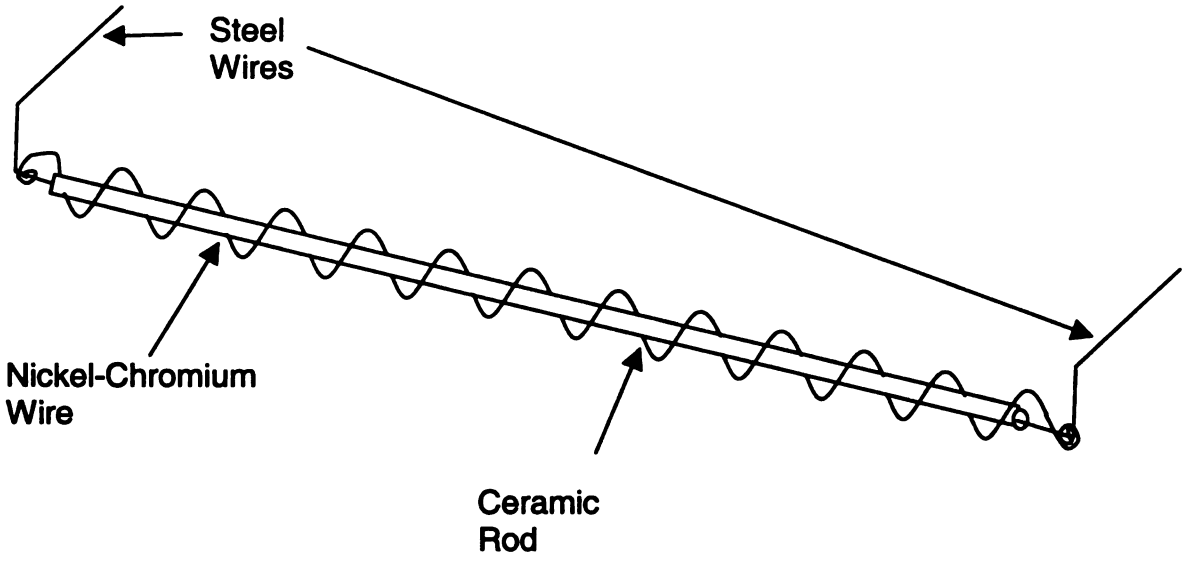

Figure 2.7 Ignition wire assembly. Placement of the ignition assembly is given in Figure 2.8.

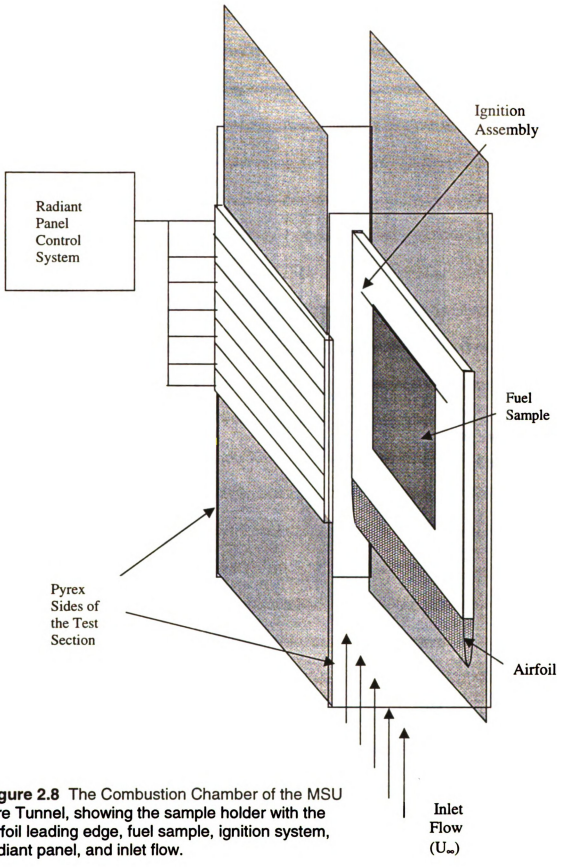

Figure 2.8 The Combustion Chamber of the MSU Fire Tunnel, showing the sample holder with the airfoil leading edge, fuel sample, ignition system, radiant panel, and inlet flow.

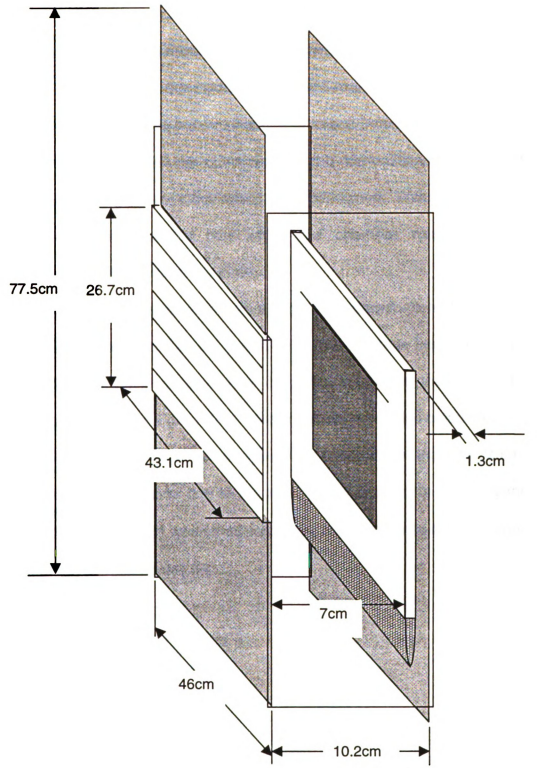

Figure 2.9 The general dimensions of the combustion chamber, showing airfoil with the sample, ignition assembly, and radiant panel.

2.4.3 Combustion Chamber Design Considerations

It is desirable for the oxidizer flow in the region between the radiant panel and the sample holder to behave like that of free stream flow over an external flat plate. In order to obtain the dimensions of the combustion chamber that would allow this, boundary layer calculations were performed. Within these calculations it was assumed that the flow within the chamber was laminar, steady, incompressible, flow over a flat plate.

By using the displacement thicknesses a determination of the desired size of the combustion chamber (H) was made. The distance from the leading edge of the airfoil to the leading edge of the sample (L_x) and the volume flow rate necessary to produce a given free stream velocity were also calculated.

Minimum chamber dimensions were sought so that the sum of the displacement thicknesses due to the sample holder and the radiant panel walls (δ^*_u and δ^*_l respectively) was small compared to the distance between the radiant panel to the sample holder (H).

$$C_q = \frac{\left[H - \left(\delta^*_u + \delta^*_L\right)\right]}{H} \qquad (1)$$

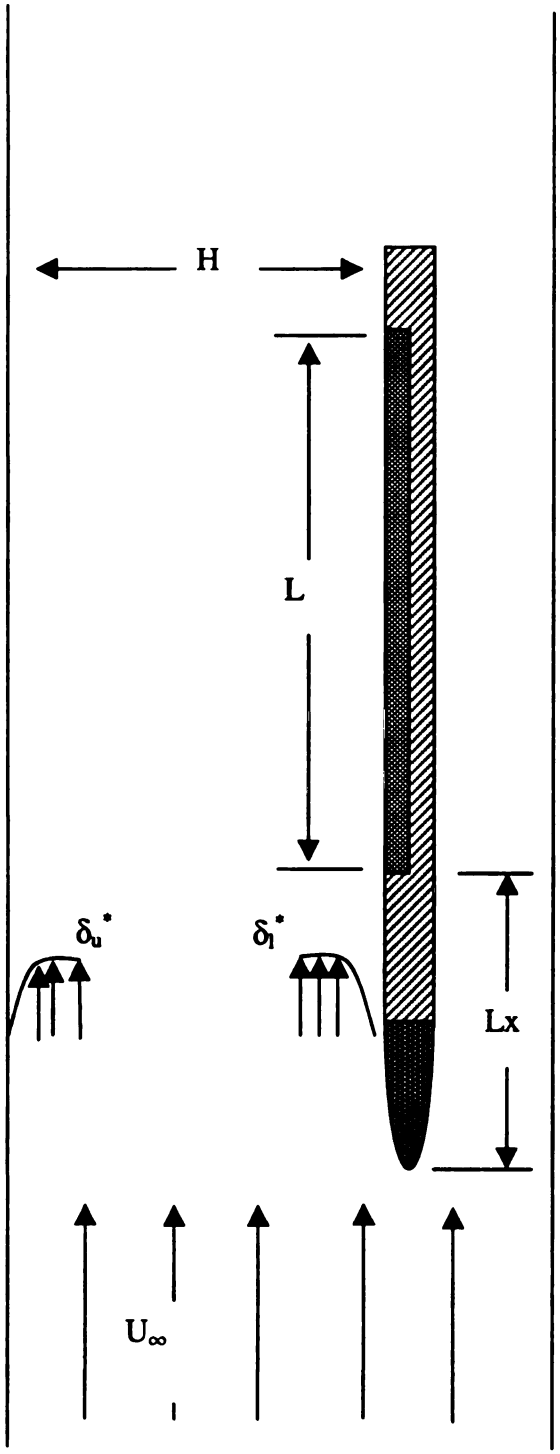

Figure 2.10 The combustion chamber, airfoil, sample holder and relevant parameters.

Equation (1) can be used to determine the effective cross-sectional area for free stream flow. C_q was chosen to be 0.88. While the choice of C_q was arbitrary, such a value ensures that the boundary layer near the radiant panel will not significantly affect the boundary layer near the fuel sample.

The leading edge of the fuel sample was used as the reference point along the length of the sample holder from which calculations were performed. By referring to figure (5) an approximation of the boundary layer thickness

$$\delta \cong 5\sqrt{\frac{\nu L_x}{U_\infty}} \quad , \qquad (2)$$

was established, where ν is the kinematic viscosity, U_∞ is the free stream velocity, and L_x is the distance from the leading edge of the sample holder to the leading edge of the sample. The velocity U_∞ was chosen to be 0.5 m/s (the lowest free stream velocity anticipated within the chamber).

Thermal expansion of the gases in the combustion chamber occurs and a correction can be made to compensate for it. The kinematic viscosity (ν) was used as the correction parameter. The fluid inside the combustion chamber was

approximated as air and the value for the kinematic viscosity of air at 1000 K was used in equation (2).

The distance from the leading edge of the airfoil to the leading edge of the fuel sample (L_x) was then determined using (2). It is desirable for the boundary layer thickness to change as little as possible over the length of the fuel sample. The difference in thickness is minimized as the sample is moved downstream with respect to the leading edge of the airfoil. Size constraints prevent this distance from being too large so a compromise was reached. The percentage differences between the boundary layer thicknesses at the trailing and leading edge of the fuel sample for a U_∞ of 0.5 m/s and a fuel sample length of 23cm for various sample positions with respect to the airfoil are given in Table 2.1.

Position of fuel leading edge (Lx) (cm)	B.L. thickness (leading) (cm)	B.L. thickness (trailing) (cm)	Percentage difference
5	0.61	1.42	57.0
10	0.86	1.54	44.1
15	1.06	1.66	36.3
20	1.22	1.77	31.0
22	1.28	1.81	29.3
25	1.36	1.87	27.1
30	1.49	1.97	24.0

Table 2.1 Calculated percentage differences between the boundary layer thicknesses at the leading and trailing edges of a 23cm fuel sample, U_∞=0.5 m/s.

From this table, a distance of 22cm gives a percentage difference between the boundary layers of less than 30%. This choice of less than a 30%

difference though arbitrary, represents a compromise between size constraints and the need to make the flow over the fuel sample as regular as possible.

Once L_x (Fig. 2.10) is known it fixes the boundary layer thicknesses and the displacement thicknesses for a given U_∞ for both the fuel sample wall and the radiant panel wall. It was assumed that the radiant panel wall has the same boundary layer behavior as the fuel sample wall (inexact, but adequate for this calculation).

$$\delta^* = \frac{1.73}{5}\delta \qquad (3)$$

Using (1),(2),and(3), the distance H between the fuel sample wall and the radiant panel wall can be calculated. H= 7cm was obtained.

The general design of the sample holder within the combustion chamber (Fig. 2.10) is credited to [12]. Modifications were made from the original design and are discussed in greater detail in section 3.1.

2.4.4 Radiant Panel

The radiant panel consists of seven OT-1801 Omegalux resistive strip heaters with an iron oxide finish. The strip heaters are mounted to a rigid aluminum frame and coated with a low gloss, black, high temperature paint. Each strip heater requires approximately 8 amps of current in order to achieve

full power. This paint enables the surface of the strip heaters to be approximated a blackbody radiator ($\varepsilon \approx 0.95$). This frame fits into tracks cut into the frame of the combustion chamber. This was done to allow the radiant panel to be rapidly slid in and out of the combustion chamber in order to avoid any power up phase of radiant sample heating.

A control system was constructed for the MSU Fire Tunnel. The strip heaters are controlled using a CN9120A Temperature Controller. A closed loop control scheme is used (Figure 2.13) with "E" type thermocouples used for temperature monitoring. The thermocouple is mounted to a strip heater with Omegabond 300 to produce good thermal contact and high electrical resistance. Four circuits are controlled with the temperature control unit using four DC input/AC output solid state relays (SSRs). One of the SSRs is an Omega SSR240DC75 with a load current capability of 75 amps. The remaining three SSRs are Crozet Gordos GA5-6D25 with load capabilities of 25 amps each. All four SSRs can be controlled with a pulsed DC current between 3 and 32 volts. One circuit is powered with a 125 Volt 15 amp line. The 15 amp line was used because only one strip heater is connected to it and because the lab only has three 30 amp lines. This 15 amp circuit powers one strip heater and is controlled via the SSR. The remaining six strip heaters draw power from three 125-Volt 30-amp lines and are also controlled with SSRs. High temperature wire connects the SSRs to the strip heaters. High temperature ring terminals were used to secure the high temperature wire to the strip heaters. The 30-amp lines come in from a three way disconnect box with slow blow 25-amp fuses. Each 30-Amp

line then has a second "fast blow" fuse in the control box. The 15-Amp circuit has a 10-amp fuse.

The Temperature Controller provides a DC pulse to operate the SSRs. Each SSR has a control side impedance of 1000Ω with a minimal voltage requirement of 3 Volts DC. The Temperature Controller can produce 5 Volts DC (pulsed) at 25mA. By connecting the SSRs in parallel (Fig. 2.11), the resistance "seen" by the temperature controller becomes smaller. The combined impedance is 250Ω and the minimum current necessary to switch the SSRs is 20mA, 5mA lower than that provided by the Temperature Controller (5mA margin of safety).

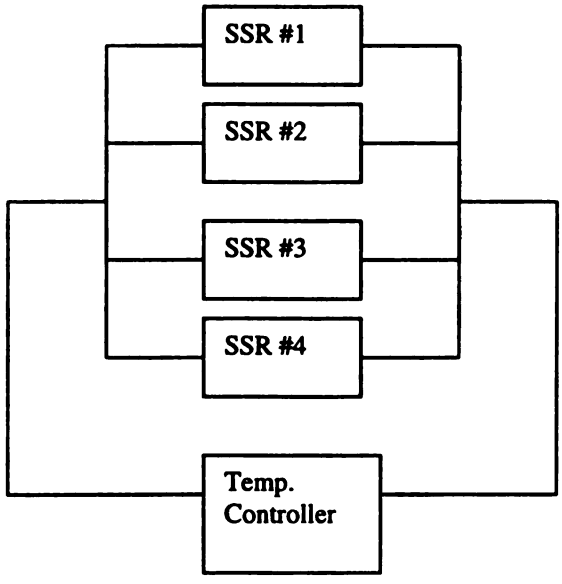

Figure 2.11 Control side wiring of the SSRs, which are connected in parallel in order to reduce the overall resistance required by the temperature controller to control the system.

During operation the SSRs will heat up. For this reason they are mounted to finned heat sinks. The SSRs and the rest of the control system is mounted within a metal enclosure that has a fan (capable of delivering 30 CFM) to provide cooling.

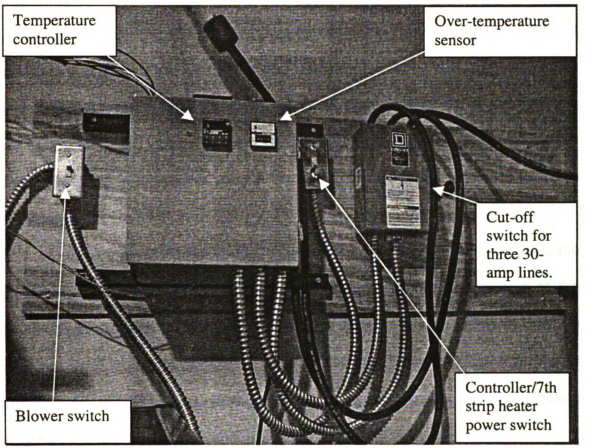

Figure 2.12 The control system for the MSU Fire Tunnel.

The design of this control system has an inherent danger. Seven strip heaters are controlled yet only one is monitored. It is possible (however unlikely) that the strip heater that is being monitored could burn out. This would fool the control system into treating the strip heaters as if they were cooling, thus causing a possible overheat situation. Therefore as a safety precaution, a separate over-temperature sensor has been included in the control system (not included in Figure 2.13).

A CN355-KF High Limit Controller monitors the temperature of the radiant panel via a thermocouple (again bonded to a strip heater with Omegabond 300). The CN355-KF has a trip light on it. If the measured temperature exceeds the set temperature the green light will go off. It can be connected to an audible alarm designed to signal the user in the event of an over-temperature potential emergency.

Once the control system and radiant panel were constructed and in place an auto-tune feature was used to optimize the PID control parameters of the Temperature Controller. The controller goes through a succession of heat up and cool-down cycles to determine the system characteristics. This algorithm is built into the controller and needs to be performed only once. The parameters obtained are stored in the controller even when the power is turned off.

2.5 Exhaust Hood

The exhaust hood is positioned downstream of the outlet of the combustion chamber and hangs from four chains secured to overhead supports. The steel exhaust hood is 91.5cm x 91.5cm at its inlet and 61cm deep. A 12.7cm diameter round pipe extends from the exhaust hood to an overhead duct that leads to a separate chemical hood. When the fan on the roof of the building is turned on the glass slide for the chemical hood must be closed in order to achieve the desired flow rate in the exhaust hood. The round duct extending from the exhaust hood is fitted with a butterfly valve in order to shut off the flow and increase the flow rate to the chemical hood.

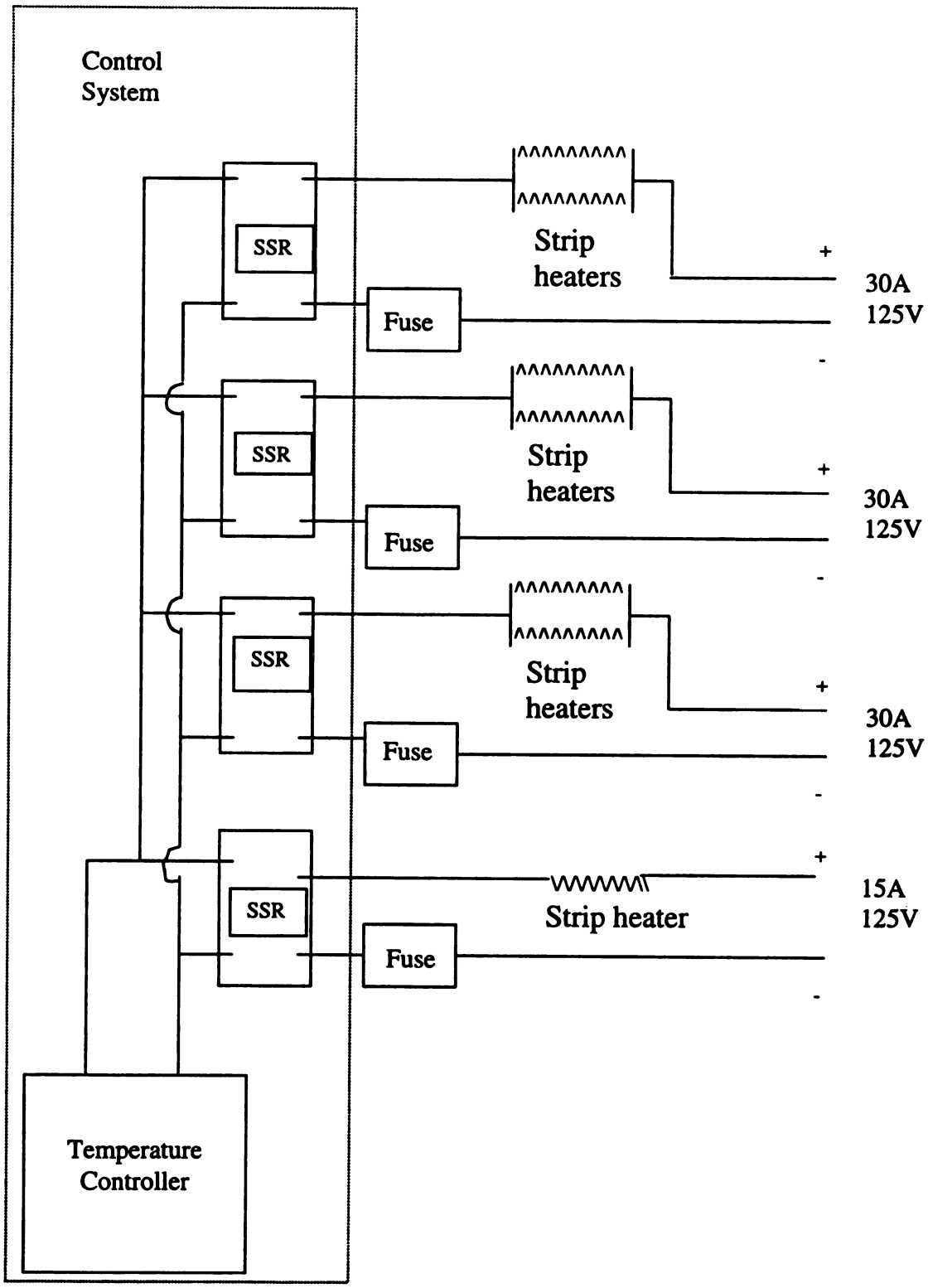

Figure 2.13 Basic outline of the radiant panel control system.

CHAPTER 3

TEST METHODOLOGIES AND DATA ACQUISITION TECHNIQUES

Tests on various components of the MSU Fire Tunnel were performed. Because this is a brand new experimental apparatus, considerable time was also spent refining the flame spread test methodologies and the geometrical configuration of the test section. Ultimately, full-scale flame-spread tests were performed and the flame-spread rates were recorded.

3.1 Various Experimental Configurations Tested

In the process of refining the experiment a variety of experimental configurations were tested and examined. Changes (from what was initially built) were made to the elbow meter, the inlet to the settling chamber, and the sample holder. A fin attached to the trailing edge of the sample holder was tested and eventually not used for flame spread tests (for practical reasons).

Initially, the PVC pipe leading from the blower to the elbow meter contained three pieces of honeycomb and four wire cloth sections placed within it to suppress turbulence. It was found that the blower could not produce the desired free stream velocity within the combustion chamber with these pieces in place, so all but one piece of honeycomb was removed.

Another part that was tested was a diffusion pipe within the settling chamber. As air entered the settling chamber it passed through a pipe with a

series of holes in it designed to diffuse the initial momentum of the incoming air over a larger area. Again, it was found that this impeded the blower to the degree to which it could not produce the required free stream velocity within the combustion chamber.

Several refinements were made to the sample holder and the type of sample used. The sample that was used for the first flame-spread test was a piece of molded thermo-set acrylic 6.4mm thick. When this sample was exposed to heat it did burn; it also melted and dripped into the combustion chamber. It was found that the use of cast acrylic is the standard for flame spread tests and cast acrylic was used in all subsequent flame spread experiments.

The first few flame-spread tests were done with 6.4mm thick cast acrylic mounted in the Marinite board. The first Marinite sample holder was had the same dimensions as the one described in Chapter 2 but differed in the space that the fuel sample was mounted. A 1.3cm gap was left between the back of the sample (the side not exposed to the radiant flux) and the aluminum sample holder tray. As flame spread occurred over the surface, the fire would creep around to the back of the sample and not only ruin the structural integrity of the sample but also create irregular surface flame fronts.

A new Marinite sample holder board was made for a different sample thickness (1.3cm). Also the number of screws that mounted the sample was increased to nine. This solved the problems of sample sagging and flame-spread to the back of the sample. The new Marinite board was made such that a 1.3cm deep recessed region (not all of the way through the 1.7cm thick sheet)

just big enough for the fuel sample was cut in its center. The 1.3cm thick sample was placed into this void.

Flow profile and flame spread tests were also performed with a fin mounted to the sample holder. While Figure 2.10 depicts the primary test configuration used, an alternate test configuration was also utilized. The design for this configuration was the original design discussed in [12]. A fin was placed on the back end of the sample holder (Fig. 3.1).

Because the sample holder is offset with respect to the centerline of the combustion chamber the pressure drop along a streamline on the front of the sample holder is different than on the back of the sample holder. It is thought that this moves the hydrodynamic stagnation point from the tip of the airfoil to some location behind it (near the back wall). This may be one of the causes of non-uniformity in the free stream velocity profile over the sample holder.

Use of the fin at the trailing edge of the sample holder has proved to be problematic during flame spread tests. A first version of the fin was made from 0.8mm thick aluminum sheet and was secured on the trailing edge. Fire entered the gap between the fin and the sample holder burned a hole into it.
A second fin was made from 1.6mm thick aluminum but similar problems occurred. While it is not clear that the presence of the fin significantly affects flame-spread, further study of this issue is recommended.

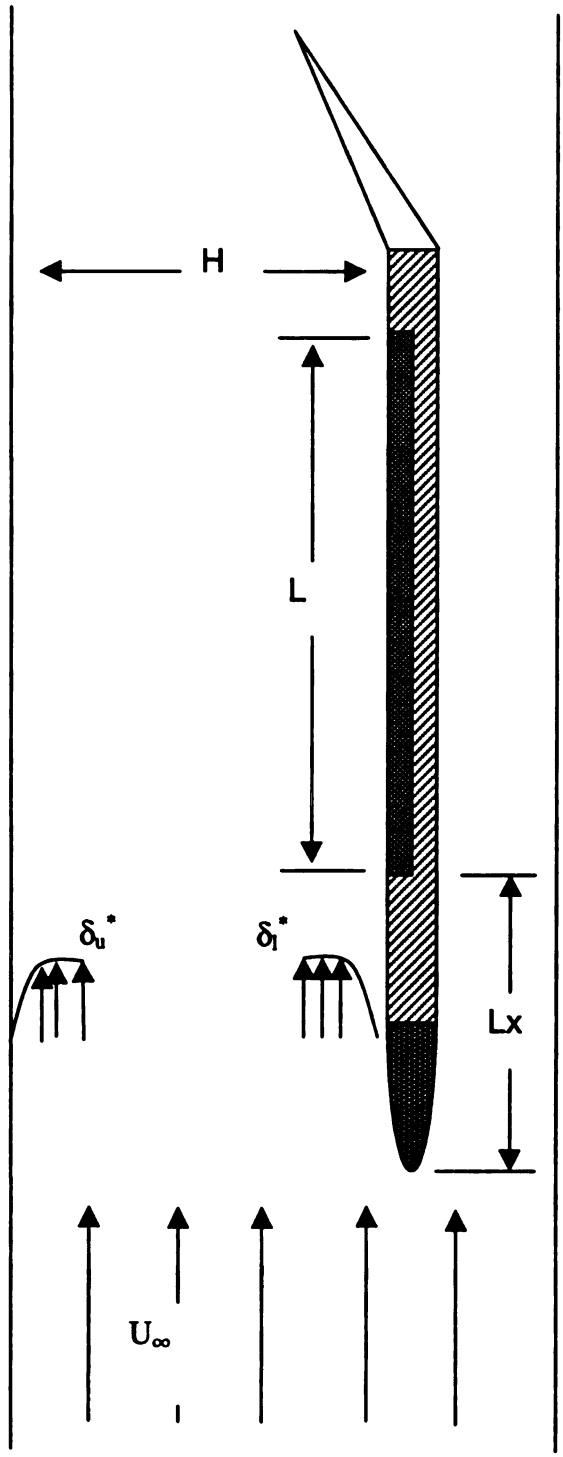

Figure 3.1 The sample holder including the fin on the trailing edge.

3.2 Component Testing

The first of the components tested were the contraction and conditioner. Flow profile testing of the contraction was done to verify that the velocity profile was uniform at the outlet. It is desirable for the leading edge of the airfoil to be situated in the free stream flow. Therefore, the thickness of the boundary layer at the outlet of the converging duct determines the minimum distance that the sample holder can be placed with respect to the combustion chamber wall. For this reason, tests were performed to obtain an estimate of the boundary layer thickness at the contraction outlet.

The velocity profile was measured across the short dimension of the converging duct outlet using a pitot tube probe and manometer. The outlet of the converging duct was fixed to a plenum held at a pressure lower than atmospheric. This test configuration included the flow conditioner, which was attached to the converging duct at one end and left open to ambient air at the other end (Fig. 3.2).

Another component tested was the ignition wire system. Nickel-Chromium wire was wrapped around short lengths of ceramic rod and placed near small PMMA samples.

In order to make ignition at the trailing edge of the fuel sample uniform, several parameters were adjusted until it was found that ignition was insensitive to their effect. The voltage per unit length of ignition wire, the spacing between

successive wraps and the proximity to the sample were varied until it was found that there was spanwise uniformity in ignition.

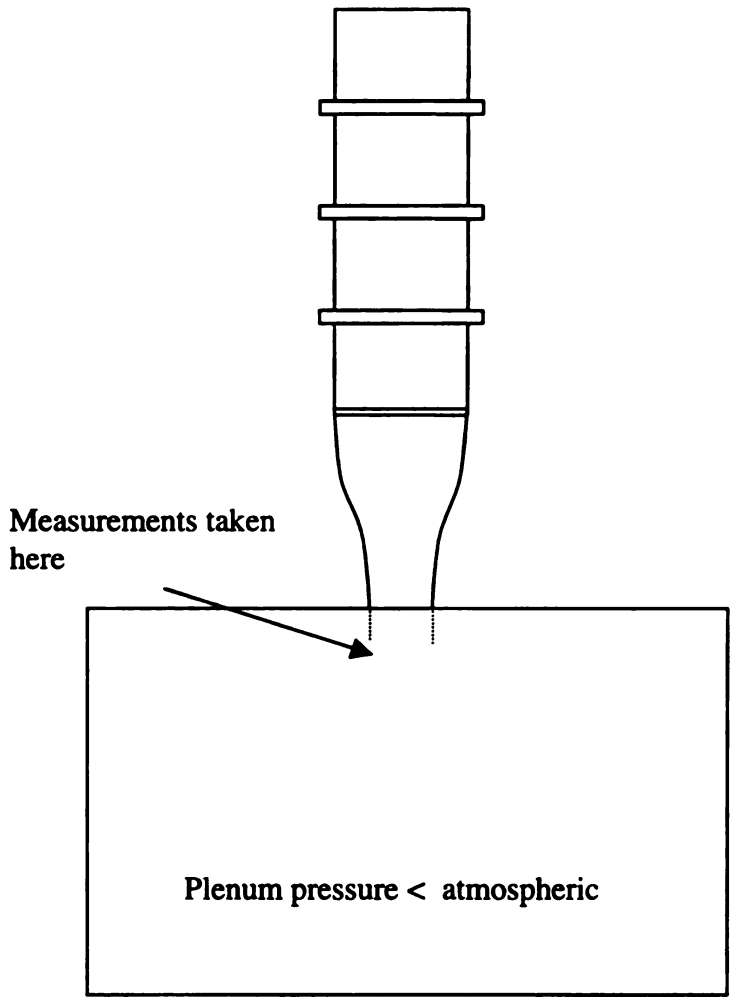

Figure 3.2 The configuration for the contraction/conditioner component tests.

The next component tested was the radiant panel. Spatial variations in the surface temperature of the strip heaters will occur due to manufacturing inconsistencies, surface emmisivity variations, and conduction losses. This, in

turn, will cause variations in the surface heat flux. Thermal imaging of the radiant panel was performed in order to characterize this variation. Additionally, any discrepancies in temperature between that measured by the control system and that measured by the thermal imaging camera were sought.

An Inframetrics 600L infrared camera capable of measuring infrared radiation wavelengths between 8 and 12 microns was used to image the radiant panel surface. In order to minimize natural convection the radiant panel was oriented such that it was horizontally with respect to the ground. Additionally, 8cm long baffles were secured along the edges to inhibit airflow around the edges of the radiant panel. Images were taken at two different temperatures and recorded on a VCR. Image processing software (ImagePro 3.0) was used to pseudo-color the images.

The effective heating area was determined using the image processing software. The software was spatially calibrated using structures recognizable in the thermal image (i.e. lines that exist on the image were recognizable on the thermal image and represent the junction between successive strip heaters). The distance between the outer edges of four of the strip heaters is known to be 15.3cm and this was used as a calibration. Next, the length and width of the region within the thermal image that fell within the measured range of the camera was measured.

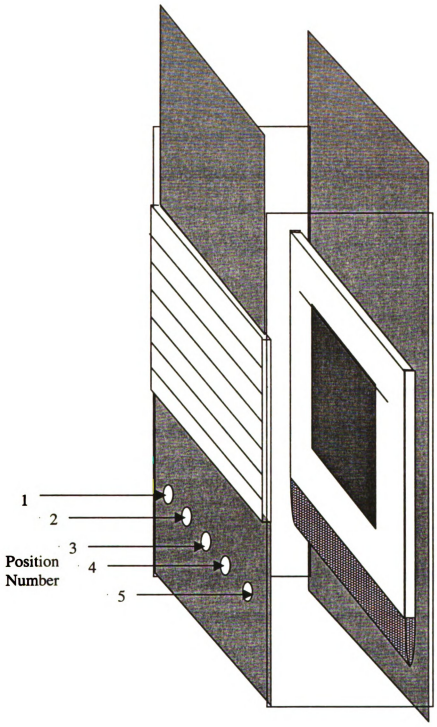

Figure 3.3 Locations of hot wire probe traverses.

3.3 Combustion Chamber Flow Measurements

Tests of the velocity profile in the combustion chamber were performed under the standard operating configuration (MSU Fire tunnel Fig. 2.1). Point measurements of the velocity within the combustion chamber were taken with a TSI IFA 300 Constant Temperature Anemometer. The data-sampling rate was 2000 Hz and 16 Kpts were collected for each probe location. Thus each data point represents the average of 16,384 velocity measurements. Thermal Pro software was used to enable the calculation of the turbulence intensity to be made from the velocity data. The hot wire probe was traversed across the width of the test section between the sample holder and the radiant panel.

The probe was inserted into holes cut in a panel just below the strip heaters. Five such holes were drilled, thus enabling data to be gathered at five different spanwise locations in the oxidizer flow.

3.4 Flame-Spread Tests

Flame-spread tests were conducted within the combustion chamber. The purpose of these tests was to determine the relationship between the set radiant panel temperature and the flame-spread rate. Secondary goals were to determine the repeatability of the tests and to gain an understanding of the general nature of the test apparatus.

The test apparatus was set up in the configuration described in Chapter 1. No fin was used in these flame-spread tests. A PMMA fuel sample was mounted

in the sample holder and the ignition wire was placed directly on it. The blower was turned on thus setting the free stream velocity to 2.2 m/s ±0.1. The radiant panel was heated to the desired temperature and slid into the combustion chamber. A sample heat-up time of 2:00 minutes (chosen arbitrarily) was used before the ignition wire was powered up.

The entire event was filmed with a Sony CCD-TRV75 NTSC video camera from one side of the combustion chamber through the glass side. As the ignition

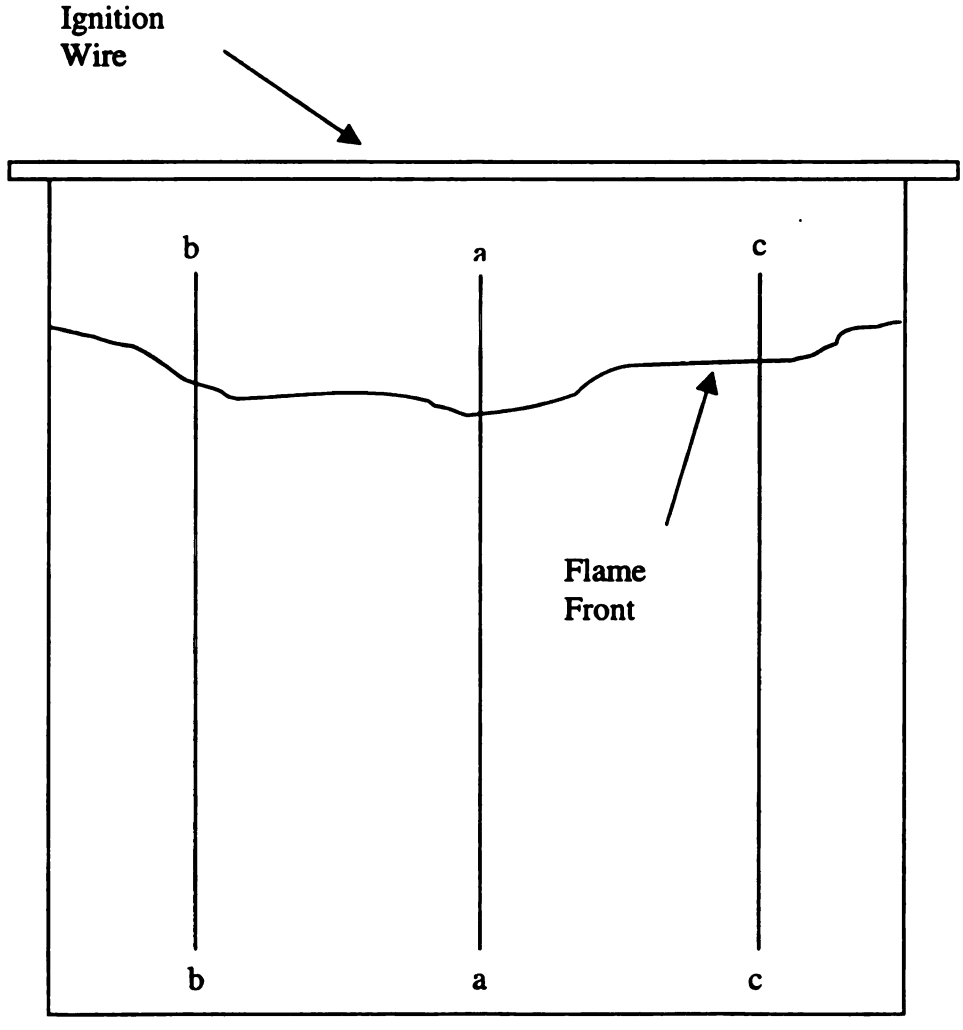

Figure 3.4 Solid fuel sample. Flame-spread measurements were made along a-a not b-b or c-c.

wire was powered up and subsequent combustion occurred, the aperture of the camera was closed in order to compensate for the brightness of the flame. The experiment continued until the entire sample burned or until 14 minutes elapsed. The flames were then extinguished using an injection of bottled Nitrogen gas.

The videotape was analyzed using the image analysis software ImagePro 3.0 to determine the rate of flame-spread over the sample surface. The software was configured to grab an image from the videotape at a constant time interval. The distance from some reference point at the top of the sample to the flame front was measured for each picture acquired.

The software enables the user to define a reference length with regard to the image. A "calibration" image was obtained and the length of the sample was chosen as the reference dimension. Using this method, each subsequent measurement on the sample can be made with respect to the defined dimension, allowing absolute measurements to be obtained fairly easily.

An origin at the top center of the sample was chosen for each test run and was referenced in terms of its pixel location. This pixel was then used as the starting point for the measurements of the flame front location. In order for this to be a valid technique it must be assumed that the camera does not move significantly during one test.

Measurements of the flame front location were made "visually", i.e. by just drawing a line from the origin pixel to the leading edge of the flame. This appears to be an inaccurate method but because the aperture of the camera was

adjusted to compensate for the brightness of the flame the difference between the flame and the fuel sample was stark and could easily be visually resolved to two or three pixels.

Measurements of the location of the flame front were always made along the centerline of the sample (Fig. 3.4). The flame fronts on the fuel surface were non-uniform in the spanwise direction but the center always spread the furthest.

CHAPTER 4

RESULTS AND DISCUSSION

4.1 Introduction

Presented are the results of the various component tests and full scale flame-spread tests. Measurements of the velocity profile at the outlet of the converging section (in a testing configuration) for various free stream velocities were performed. Tests of the flow profile in the combustion chamber were conducted with no combustion and no radiant heating. Thermal images of the radiant panel were taken. Finally, flame-spread tests were conducted at several radiant panel set temperatures.

4.2 Converging Duct Testing

Flow profile testing of the converging section was done to verify that the velocity profile was uniform at the outlet of the contraction. These tests were also performed in order to obtain an estimate for the boundary layer thickness. The error bars represent errors accumulated from uncertainties in the reading of the pressure transducer as well as errors associated with its calibration.

The Figures 4.1 through 4.4 represent measurements taken in the manner described in section 3.3. They indicate a uniform velocity profile in the bulk of the outlet of the conditioner as well as relatively thin boundary layers.

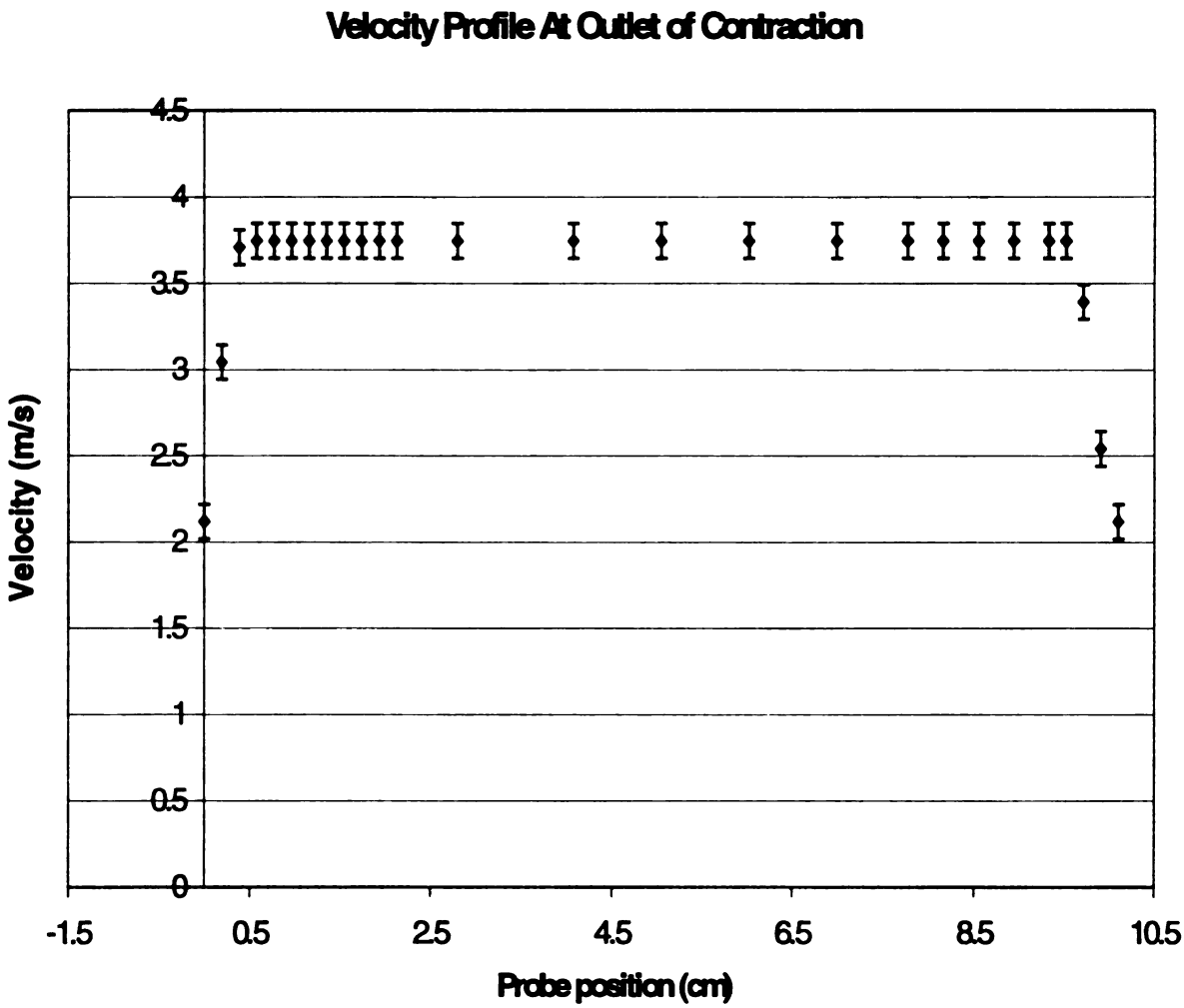

Figure 4.1 The velocity profile across the outlet of the converging duct at a bulk velocity of approximately 3.7 m/s as measured by a pitot tube. The error bars represent errors accumulated from uncertainties in the reading from the pressure transducer as well as errors associated with its calibration.

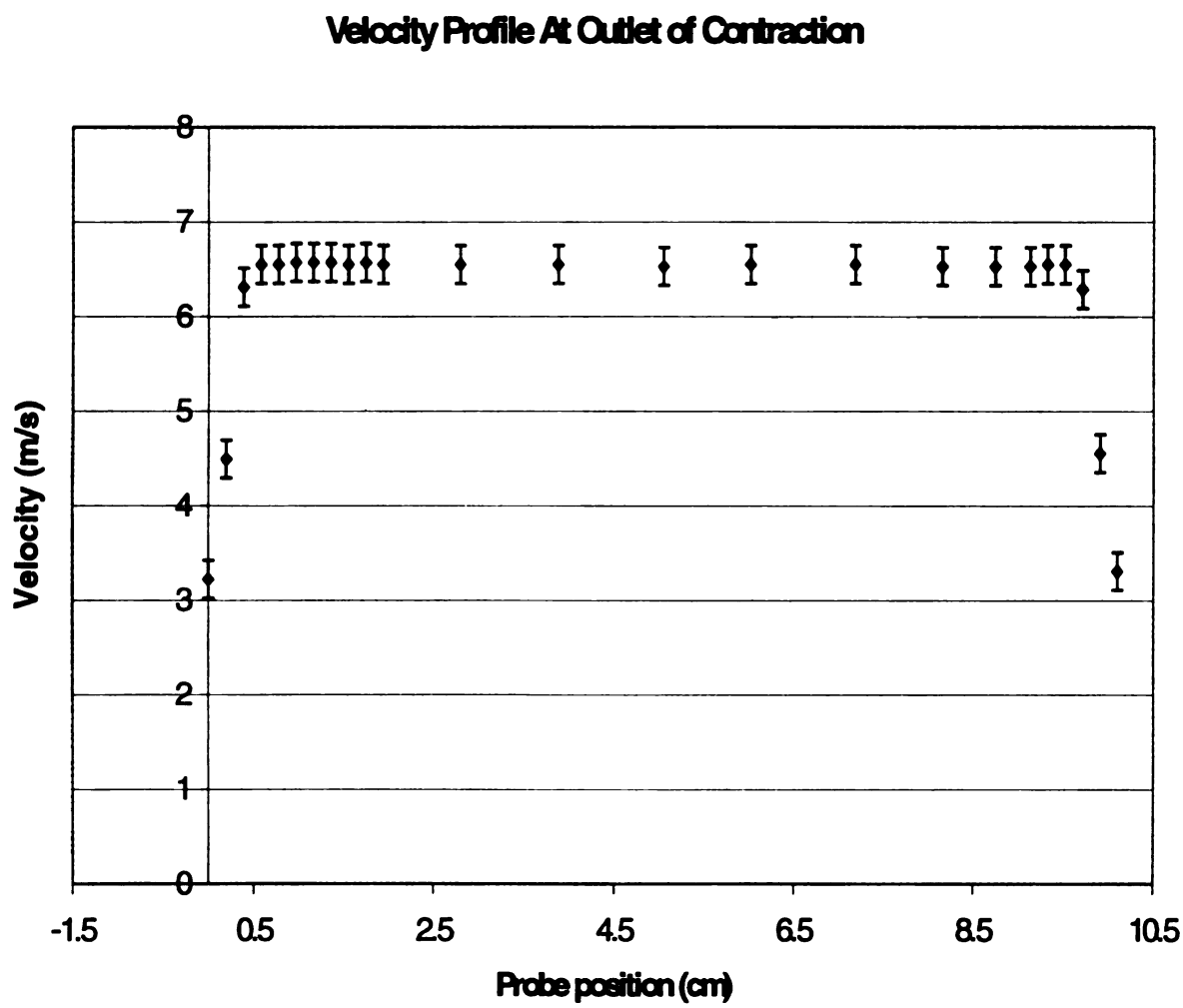

Figure 4.2 The velocity profile across the outlet of the converging duct at a bulk velocity of approximately 6.7 m/s as measured by a pitot tube.

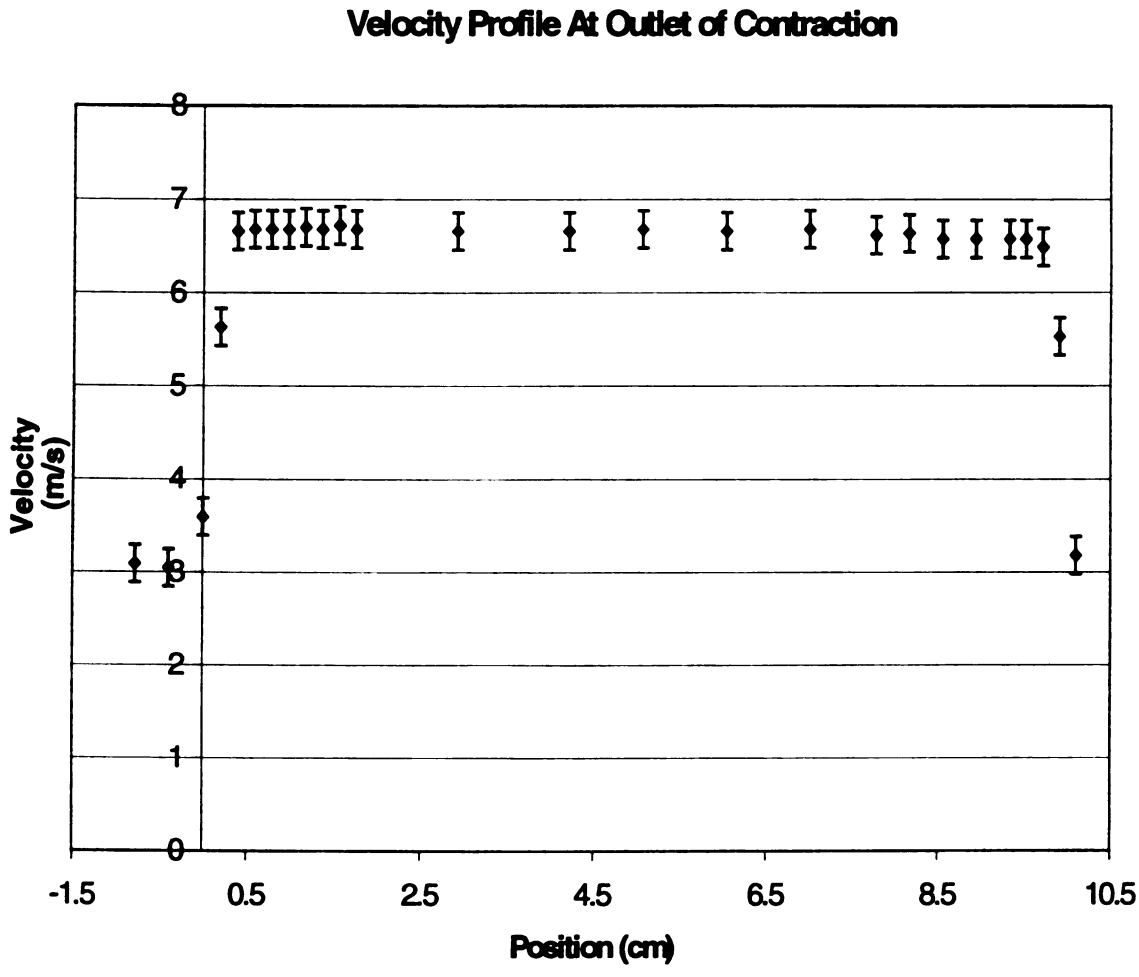

Figure 4.3 The velocity profile across the outlet of the converging duct at a bulk velocity of approximately 6.7 m/s as measured by a pitot tube.

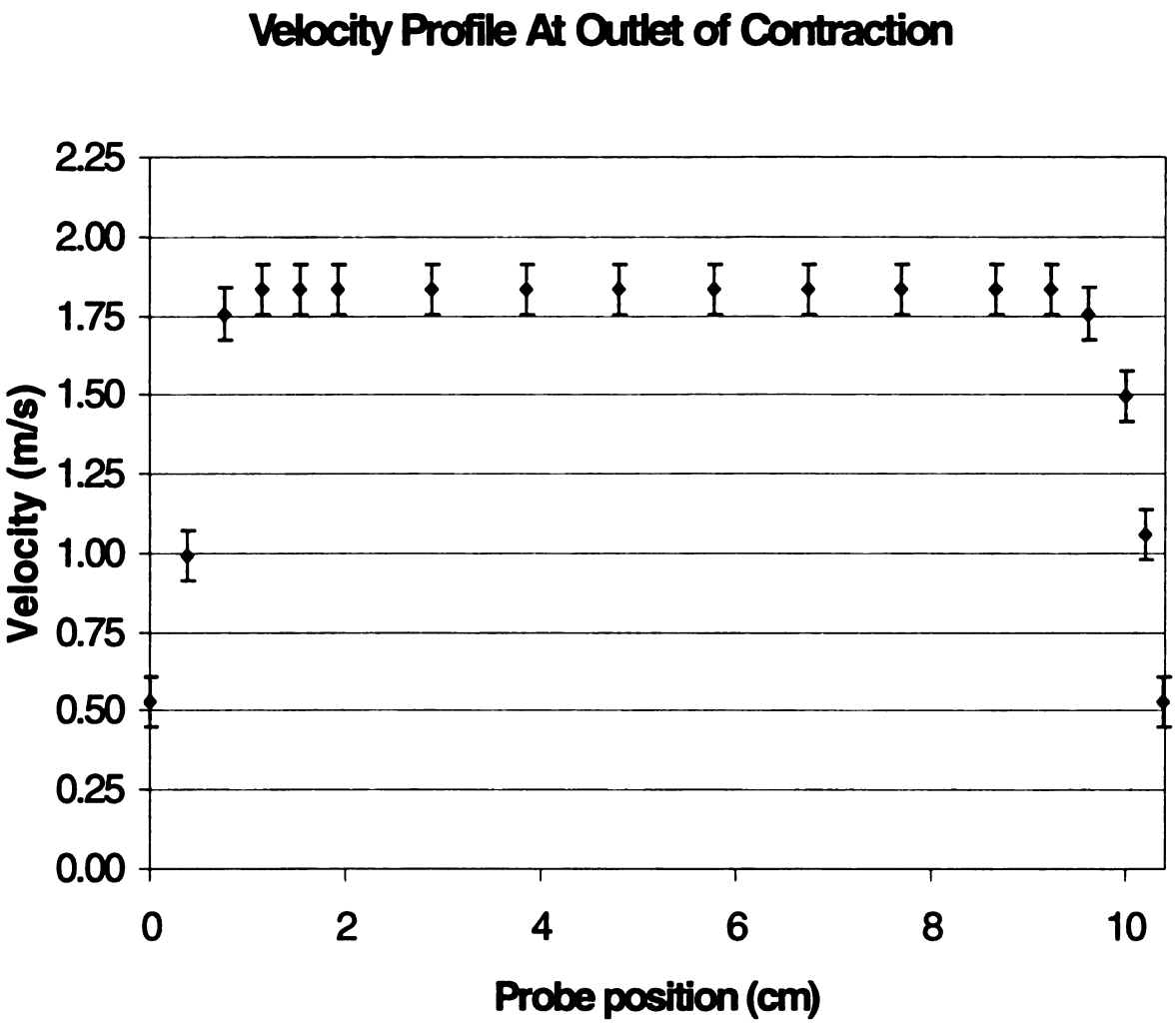

Figure 4.4 The velocity profile across the outlet of the converging duct at a bulk velocity of approximately 1.8 m/s as measured by a pitot tube.

4.3 Radiant Panel Thermal Images

Thermal images were taken at two radiant panel set temperatures (232° C and 315° C) using an infrared camera. Figure 4.5 represents the gray-scale image acquired at the set temperature of 232° C along with the dimensions. It is difficult to determine the relative intensity of the thermal radiation using a gray-scale image so a pseudo-colored image was also produced.

Figure 4.6 represents the pseudo-colored version of figure 4.5. Each color division represents 3.4° C. The highest temperature level displayed is 298° C and the lowest is 264° C. It is important to note that the camera has a finite range and everything that is blue is 264° C or lower but obviously not necessarily equal to 264° C. The camera (operating in this mode) has an error of approximately ±3° C.

Figure 4.7 represents the gray-scale image of the radiant panel set to 315° C. The dimensions are also given.

Figure 4.8 represents the pseudo-colored version of figure 4.7. Each color division represents 3.4° C. The highest temperature level displayed is 386° C and the lowest is 342° C.

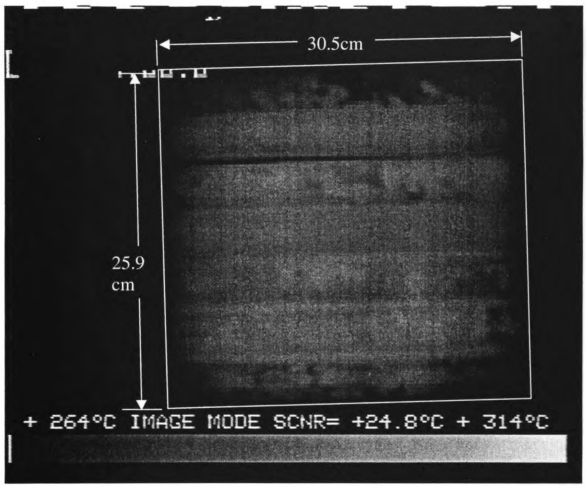

Figure 4.5 Thermal image of the radiant panel set to 232° C (gray-scale).

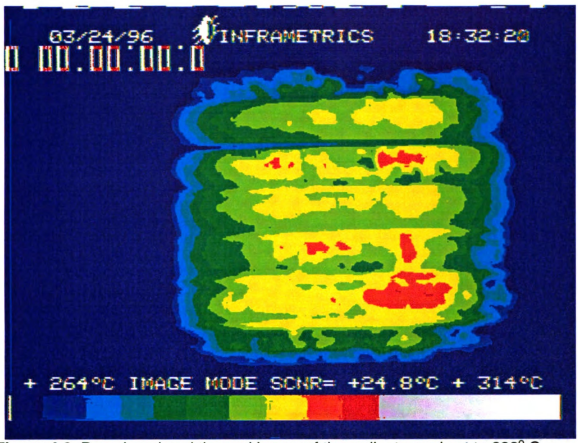

Figure 4.6 Pseudo-colored thermal image of the radiant panel set to 232° C.

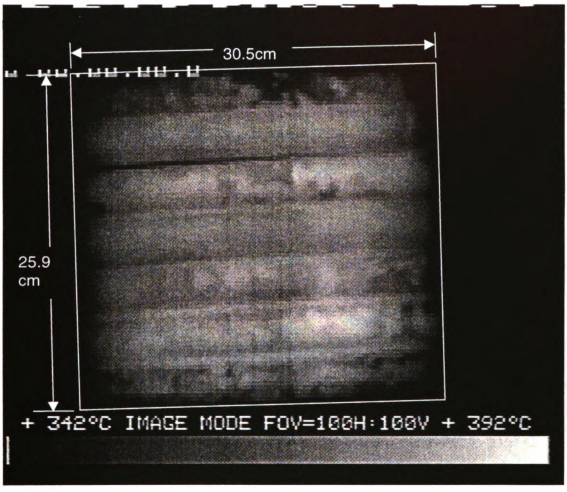

Figure 4.7 Thermal image of the radiant panel set to 315° C (gray-scale).

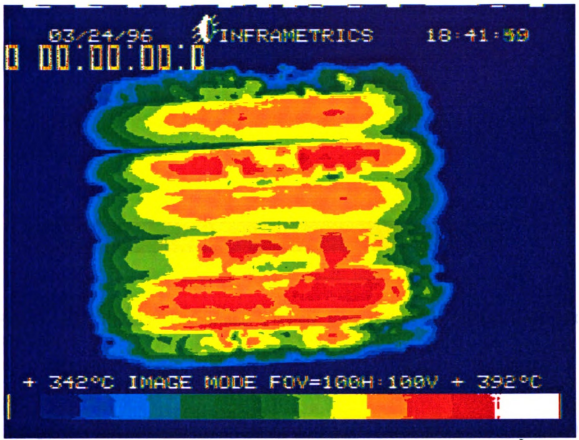

Figure 4.8 Pseudo-colored thermal image of the radiant panel set to 315° C.

In order to determine the heat flux variation across the width of the radiant panel a plot was generated for a simplified geometry (Fig. 4.9).

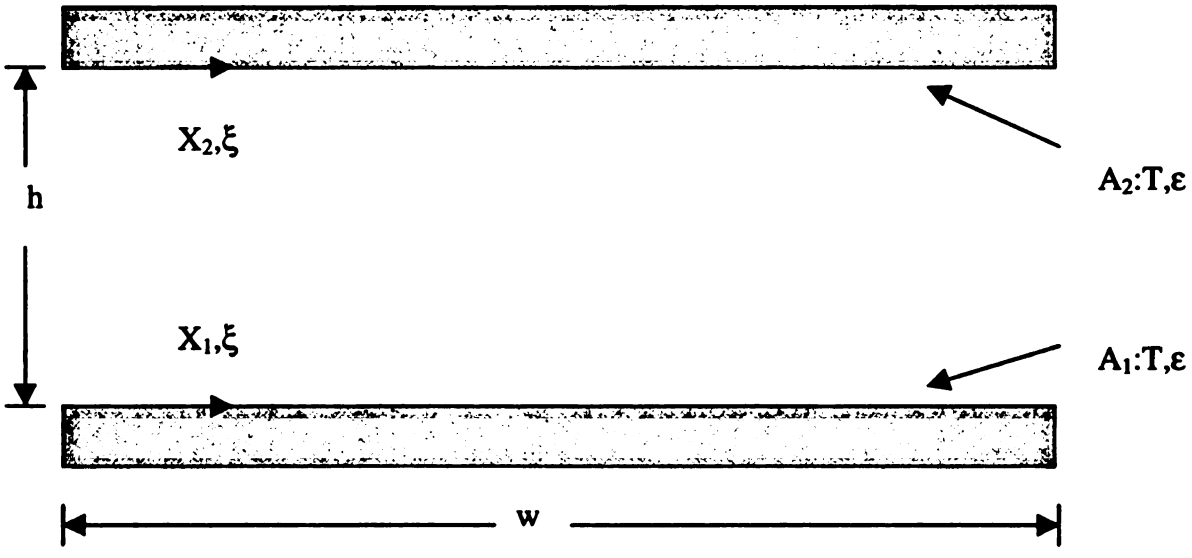

Figure 4.9 Parallel, isothermal, infinitely long plates for radiant heat flux calculation.

The geometrical configuration depicted in Figure 4.9 is solved in [15]. The system considered is a set of two infinitely long parallel plates held at a constant temperature of the same width and placed in a large, cold environment. The emssivities of the two plates are considered to be the same (ε=0.95) and in this case h = w = 1. The solution was obtained using a 1st successive approximation technique. As given in [15] the nondimensionalized heat flux loss to the surroundings, Ψ, can be represented by the following equation

$$\Psi(\xi) = \varepsilon - \frac{\varepsilon^2}{2}\left[\frac{W-\xi}{\sqrt{1+(W-\xi)^2}} + \frac{\xi}{\sqrt{1+\xi^2}}\right] - o\left[\varepsilon^2(1-\varepsilon)W^2\right] \qquad (4)$$

Where W = w/h = 1 and the nondimensionalized width parameter ξ = x/h. As $\varepsilon \rightarrow 1$ the term $o[\varepsilon^2(1-\varepsilon)W^2] \rightarrow 0$ so in this case of a "high" ε it may be discarded. Figure 4.10 represents the nondimensionalized heat flux as a function of the location along the plates.

From figure 4.10 it can be seen that the heat flux losses are greatest near the edges and minimal near the center. This calculation is obviously not a perfect representation of the true radiation problem but it represents adequately the conditions of the radiant panel. This calculation could be modified to more accurately model the problem.

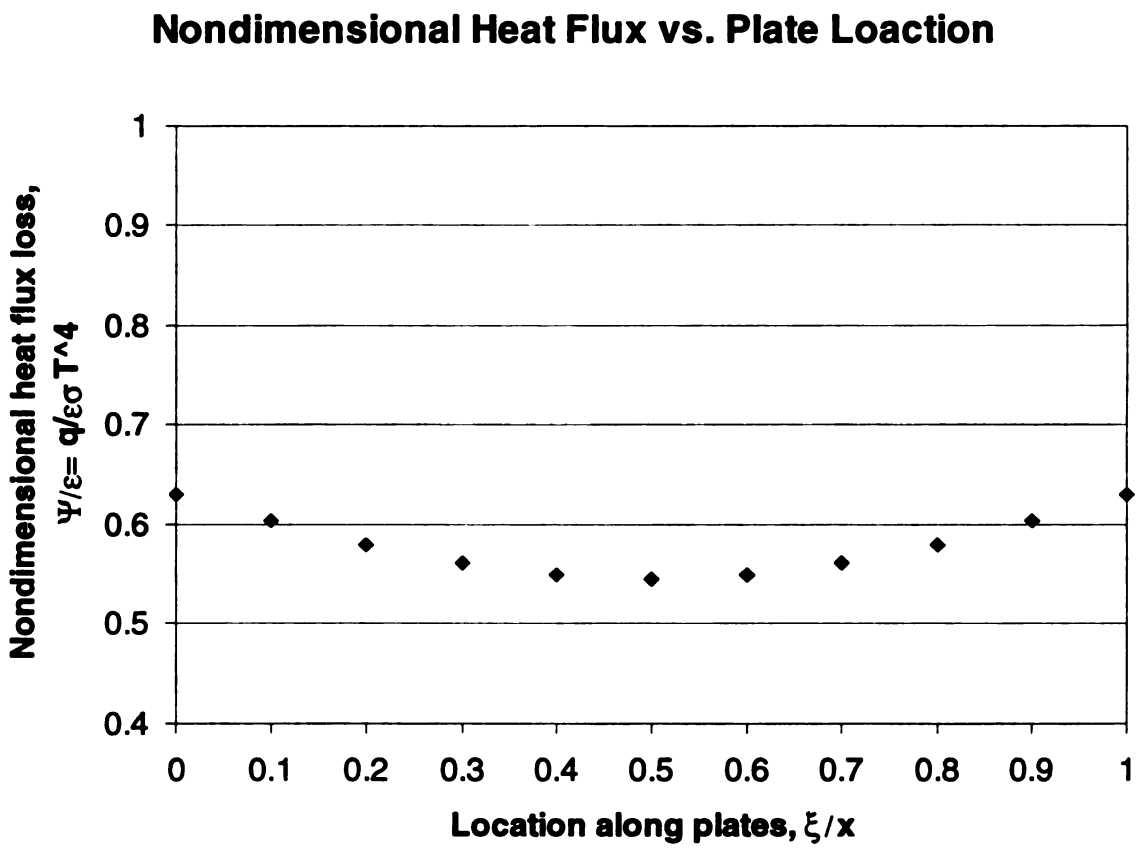

Figure 4.10 Non-dimensional heat flux vs. plate location. Note that the losses to the surroundings are the highest near the edges and that the radiant flux is the highest in the middle.

4.4 Combustion Chamber Flow Profile Tests

Tests of the velocity profile in the combustion chamber were performed under the standard operating configuration (MSU Fire tunnel Fig. 2.1). Point measurements of the velocity within the combustion chamber were taken with a TSI IFA 300 Constant Temperature (hot wire) Anemometer. Also presented are data representing the turbulence intensity across the combustion chamber.

The hot wire probe was built and calibrated using another test facility (The Ford MSU Test Facility, FMTF). The calibration was performed in a range from 2.5m/s to around 10m/s. Error can be generally estimated from these sorts of calibrations as approximately 2% when measurements are made within the calibrated range. In this case an extrapolation was made so error bars with ±4% were used.

A large number of data points (16,384) were used for each velocity data point represented on the figures. The reliability of $\bar{x}$ (the sample mean) as a measure of μ (the true mean) is $1- \sigma/(n)^{0.5}$ where σ is the standard deviation and n is the sample size [16]. This error vanishes with the sample size used.

The hot wire probe was traversed across the width of the test section between the sample holder and the radiant panel. The probe was inserted into a hole cut in a panel just below the strip heaters. Five such holes were drilled, thus enabling data to be obtained at five different spanwise locations in the oxidizer flow.

The first sets of tests were designed to determine the uniformity of the flow within the test section. These tests were conducted without the fin attached to

the trailing edge of the sample holder. Figure 4.11 represents the flow profile through the test section for this first set of tests. The zero position is at the fuel sample wall.

The measurements of the flow depicted in Figure 4.11 indicates non-uniformity in the velocity profile when no fin is attached to the trailing edge of the sample holder. This non-uniformity appears to be consistent through the width of the combustion chamber.

Next, measurements of the velocity profile in the combustion chamber were performed with the fin in place at the trailing edge of the sample holder. The fin impedes the flow and thus drops the velocity compared to the case with no fin (for the same blower throttle plate position). Figure 4.12 indicates the velocity through the test section, at position #3, for the case with the fin. Around the probe locations of about 7cm the velocities are high. Since the pressure in the combustion chamber is higher with the fin in place compared to the case with no fin (compared to atmospheric), a greater pressure differential exists. This causes a high flow velocity near the hole for the hot wire probe. Because there was no hole in the wall of the combustion chamber during normal operation, the near wall velocity data was ignored when comparing profiles with and without the fin.

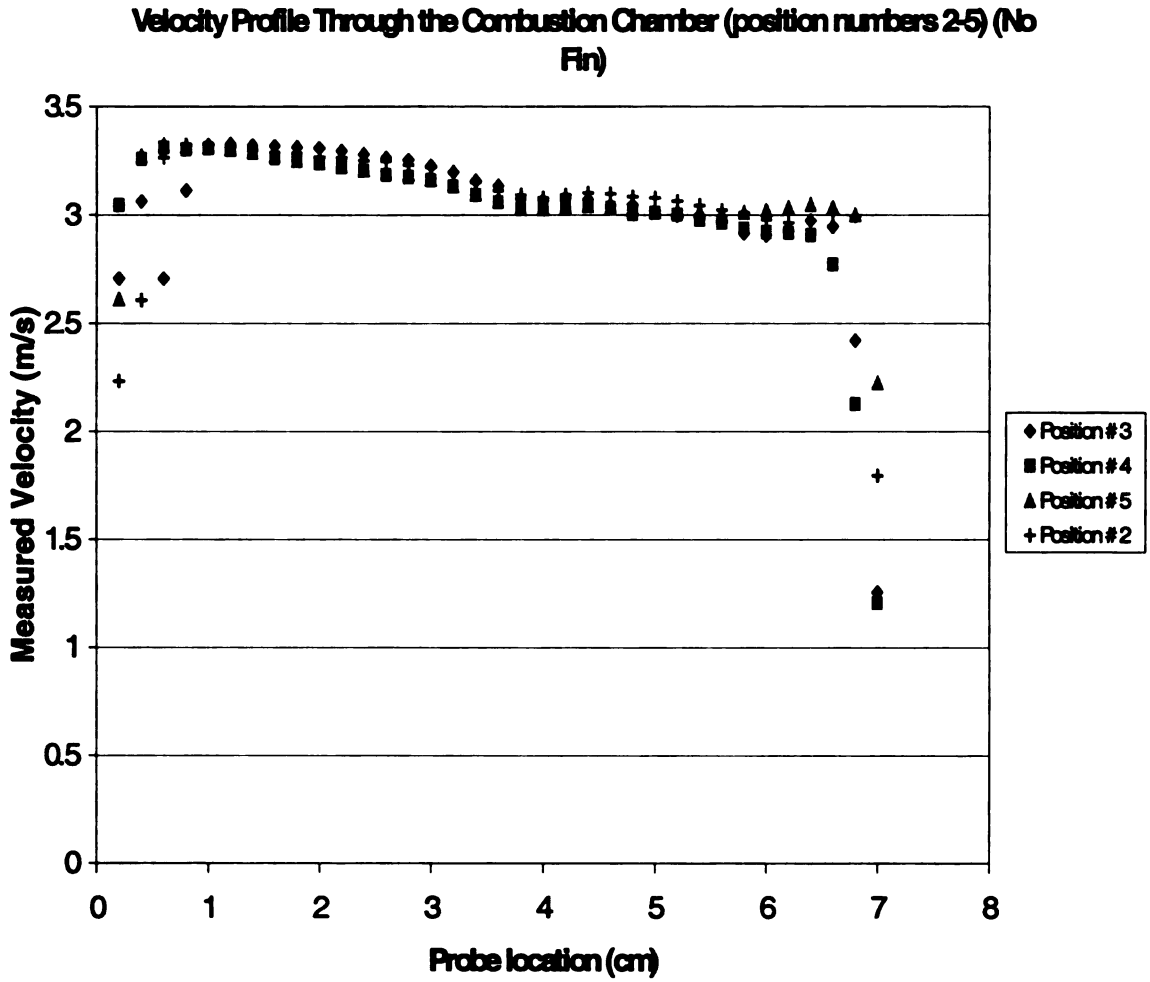

Figure 4.11 Velocity profile through the combustion chamber at four position locations, with no fin at trailing edge of the sample holder. The ±4% error bars are not displayed.

Use of the sample standard deviation of the velocity data is an effective way of determining the degree of variation across the bulk flow. The sample variances and standard deviations of the velocity through the test section for the cases with and without the fin are compared (Figures 4.11 and 4.12 for position #3). The first three and last three data points were discarded for this calculation (for both cases, with and without the fin).

	Variance	Standard deviation
Without fin	1.40E-02	1.20E-01
With fin	**1.70E-03**	**4.10E-02**

Table 4.1 The variance and standard deviation of velocity measurements through the test section with and without a fin.

There is an order of magnitude difference between the two standard deviations. The bulk velocity tested with the fin in place was lower, but this cannot account for such a large change in the standard deviation of the velocity profile. Clearly, the fin is effective for reducing variations in the bulk velocity profile.

While knowledge of the bulk flow behavior is useful, the subject of most interest is in the near-fuel region. For this reason, tests of the velocity profile near the fuel sample were conducted.

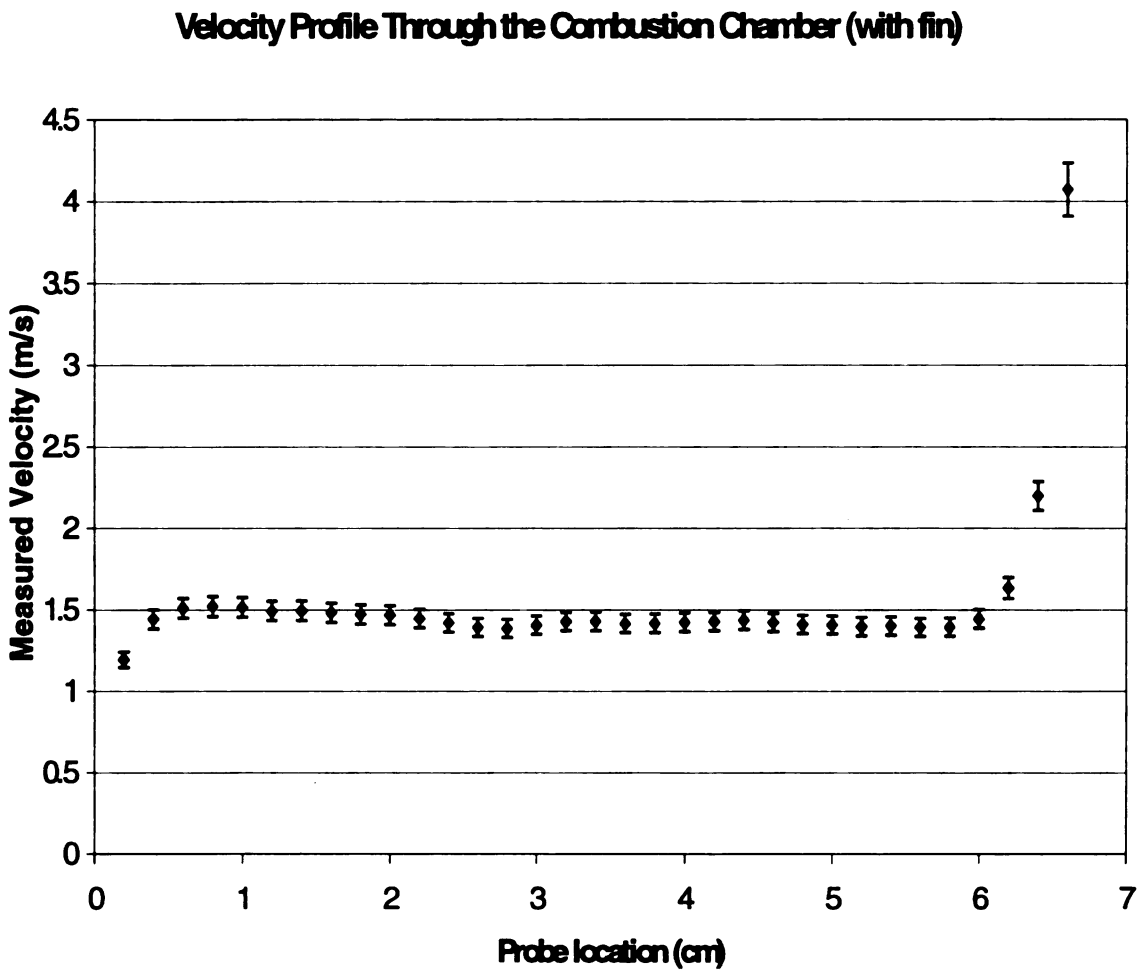

Figure 4.12 Velocity profile through the combustion chamber (position #3) with the fin.

For reasons stated earlier, the existing fin design is impractical for flame spread tests. Because of this, the near wall tests were conducted without the fin in place. A micrometer was used to achieve the fine degree of spatial resolution necessary to make measurements in the near wall boundary layer.

It must be noted that for Figures 4.13, 4.14, and 4.15 the location of the sample wall was not precisely known at the time the measurements were taken. The wall location was determined by comparing the data to the Blasius profile. Figures 4.13 and 4.14 indicate that the velocity profile is quite similar to the Blasius profile. The deviation that does exist may be due to a pressure gradient in the free-stream.

The Reynolds number based on the momentum thickness (Re_θ) was calculated at the leading edge of the fuel sample. The momentum thickness is defined as

$$\theta = 0.664\sqrt{\frac{\nu x}{U_\infty}} \qquad (5)$$

for the Blasius solution. For a free stream velocity of 2.25m/s Re_θ is 180.

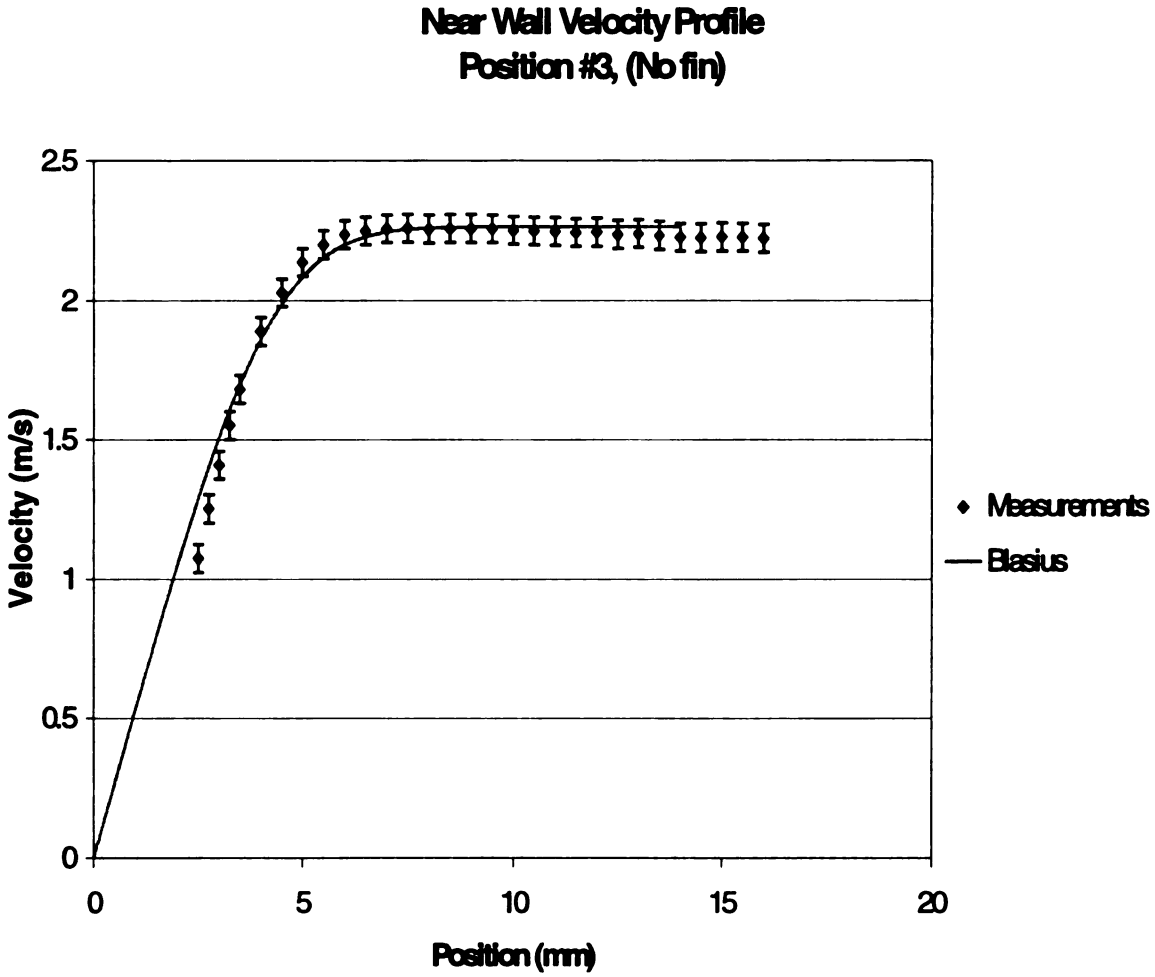

Figure 4.13 Near sample wall velocity profile, position #3, with no fin.

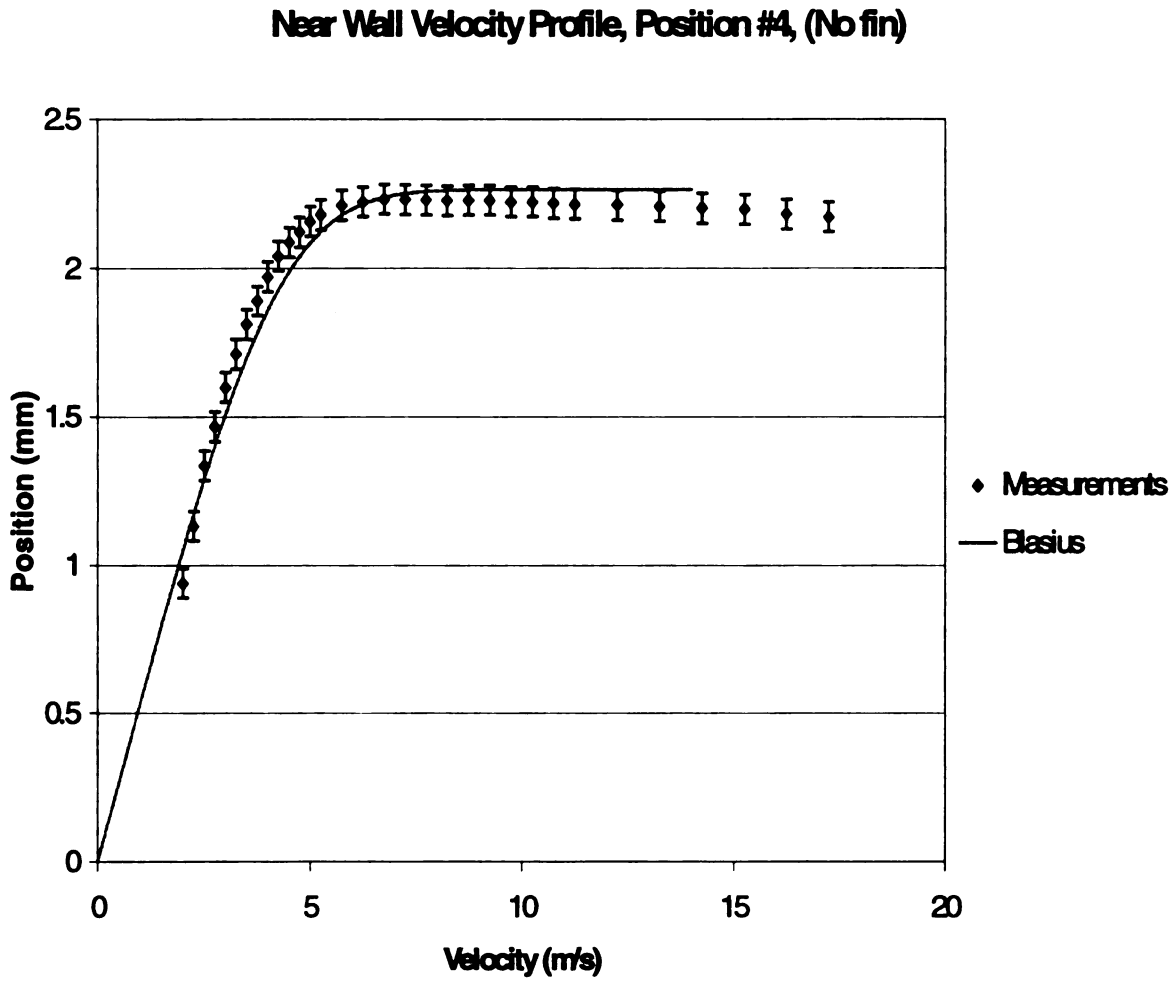

Figure 4.14 Near sample wall measured velocity profile and Blasius profile, position #4, with no fin.

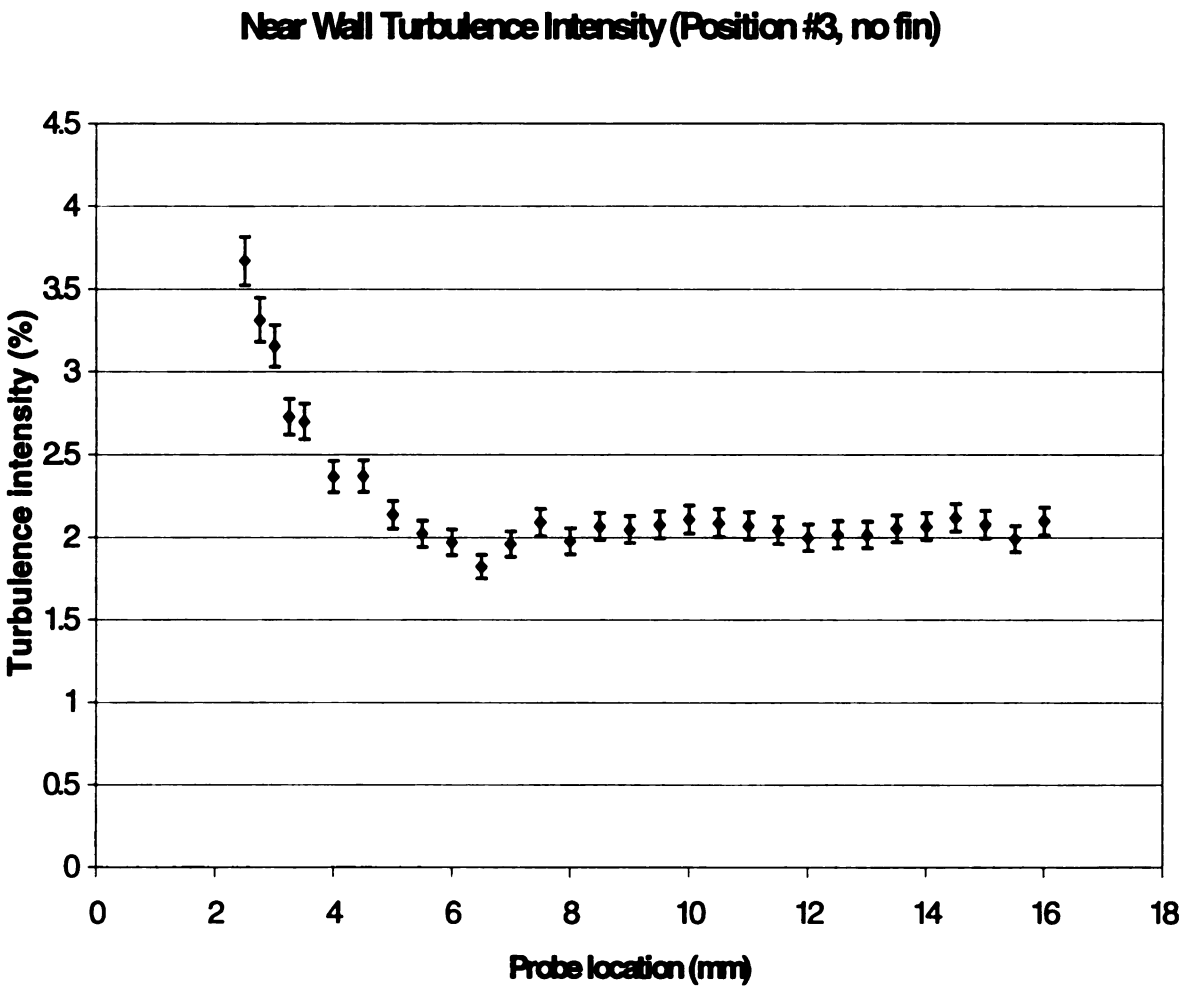

Figure 4.15 Turbulence intensity in the near sample wall boundary layer for position #3 (velocity data from figure 4.13 were used).

4.5 Flame-Spread Tests

Flame-spread tests were conducted in the manner presented in section 3.5. Presented are the results of these tests. The set radiant panel temperature was varied in increments of 50° F for the first six tests. A jump up of 100° F was taken for the seventh experiment. The remaining experiments (#8-#11) involved repeating the test for a radiant panel set temperature of 260° C in order to determine the consistency of the experiment. A least squares linear regression analysis was conducted for each experiment. The lines generated are displayed on the corresponding figures. In order to make effective comparisons the least squares line was forced to go through the origin. The equation for the linear fit and the R^2 value are displayed on each figure.

During the beginning of each test, the ignition wire was warming up and began to light the sample. Because the spatial proximity of the ignition wire to the sample surface will strongly affect the heat absorbed by the sample, variations will occur in the time to ignition. In other words, a change in ignition wire placement from one test to another as little as one millimeter will alter the time to ignition (elapsed time from when the ignition wire was turned on). Because the video data was fed into the computer at regular intervals and the first image was "snapped" when the ignition wire was turned on, an error exists in the location of the vertical axis from test to test. While this error is present in all the data it is not large and doesn't significantly affect the slope of the linear fit.

Figure 4.16 The flame front within the combustion chamber (measurement line shown).

4.5.1 Error Analysis

Error analysis was performed to determine the error in estimating the slope and intercept of the linear regression applied to the flame spread data. The standard error (S_y) can be expressed as

$$S_y = \{\Sigma_i (y_i - mx_i - b) / (M - 2)\}^{1/2} \quad (6)$$

where m and b are the slope and intercepts of the least-squares linear fit. M is the total number of measurements. The error in estimating m and b can be expressed as

$$S_m = (N / \Delta)^{1/2} S_y \quad (7)$$

$$S_b = (\Sigma x_i^2 / \Delta)^{1/2} S_y \quad (8)$$

Where

$$\Delta = (\Sigma x_i)^2 - N\Sigma x_i^2 \quad (9)$$

It was found that the errors in estimating m and b were small. Table 4.2 indicates the errors in the estimation of the slopes and intercepts of the linear

least-squares fit to the data shown in Figures 4.17 through 4.24 (excluding 4.23, where no least-squares fit was applied). The slopes that are reported in Figures 4.17 through 4.24 are given only to the significant figure that is reliable.

Experiment #	S_m	S_b
1	7.9E-05	0.16
2	7.7E-05	0.15
3	8.4E-05	0.17
4	9.0E-05	0.18
5	3.0E-05	0.05
6	8.0E-04	0.3
7	xx	xx
8	1.0E-04	0.2
9	4.0E-05	0.1
10	5.0E-05	0.1
11	2.0E-05	0.03

Table 4.2 Errors in estimating the slope and intercept of the least-squares linear fit for the flame-spread tests.

The error in resolving the location of the flame front on the pictures acquired into the image processing software was around two pixels. This translates into an error of one or two percent for each data point shown in the flame spread tests. Error bars indicating this error would be about the same size as the data point itself so they were not included.

4.5.2 Flame-Spread Test Results

Figure 4.17 (corresponding to a set radiant panel temperature of 177° C, the lowest panel temperature tested) indicates a fairly regular spread rate. It appears as though the spread rate is accelerating (with respect to the least squares fit) over time.

Figure 4.18 indicates the same general trend. The spread rate accelerates with respect to the least squares fit and then begins to level off near the end of test.

Figure 4.19 indicates the same general trend of acceleration of the flame front near the top of the sample. It can be seen clearly that this acceleration wanes and the flame front begins to decelerate. This inflection point appears to occur at around the 14.5cm point along the sample length.

Figure 4.20 displays this same general trend as the previous figures. The flame-spread rate is higher and the flame front spread further than the previous tests. The inflection point appears to be at the same point (around 14.5 or 15cm) as in the previous tests. This seems to indicate that this is a characteristic of the experimental configuration.

Figure 4.21 (corresponding to experiment #5) indicates a vigorous flame spread rate. It follows the general trend of early acceleration followed by a deceleration phase. This time the inflection point appears to have moved up to approximately 15 to 15.5cm.

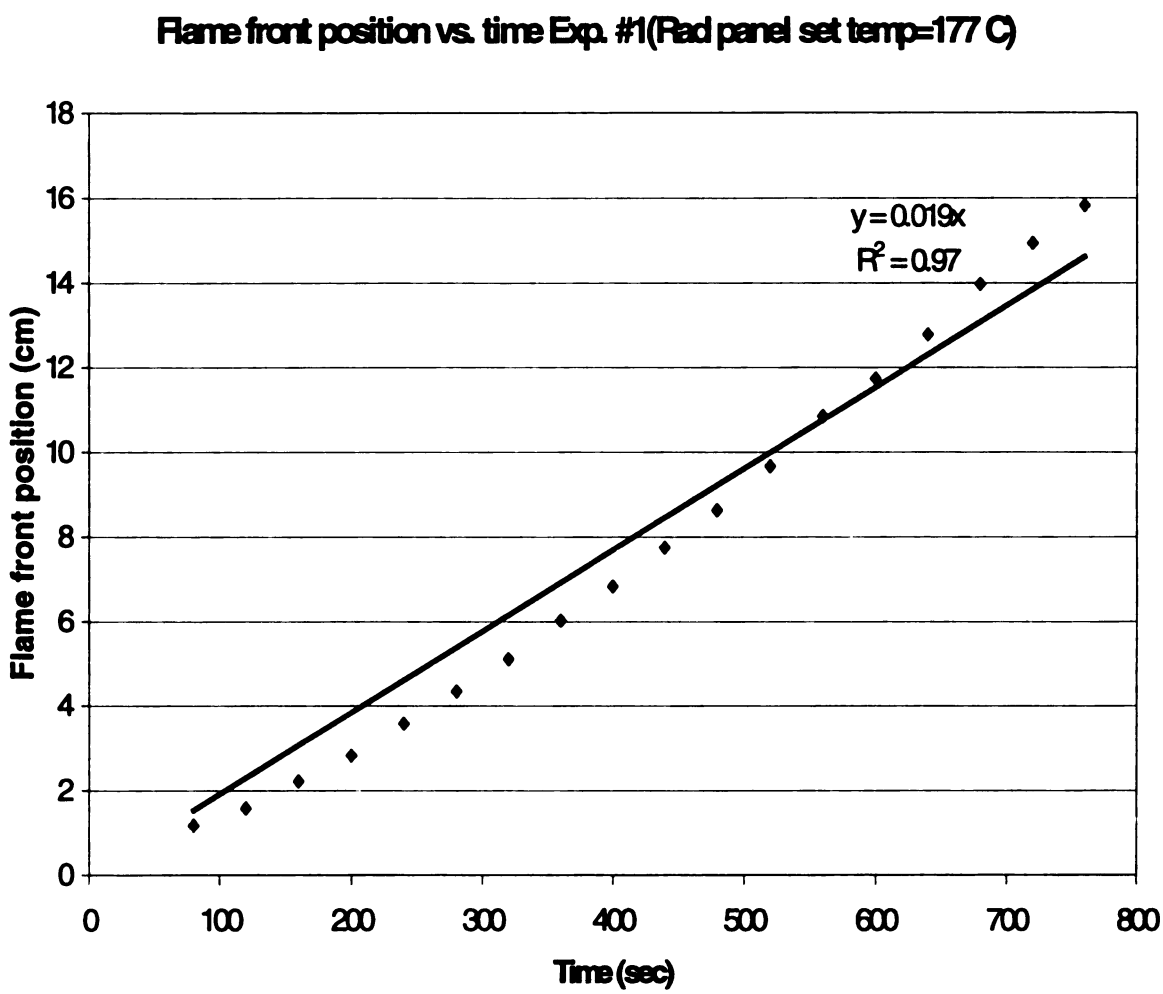

Figure 4.17 Flame front position vs. time for a set radiant panel temperature of 177° C, Experiment #1.

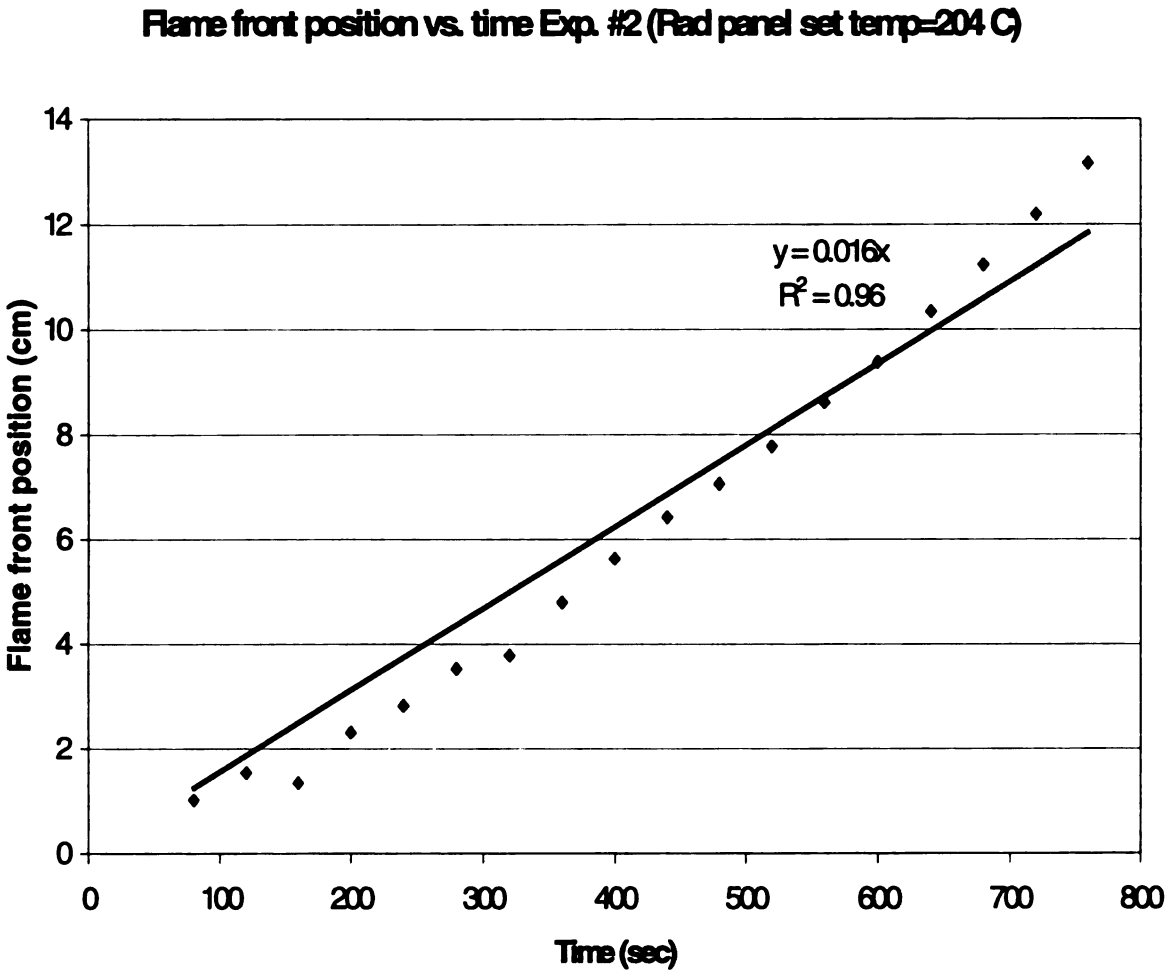

Figure 4.18 Flame front position vs. time for a set radiant panel temperature of 204° C, Experiment #2.

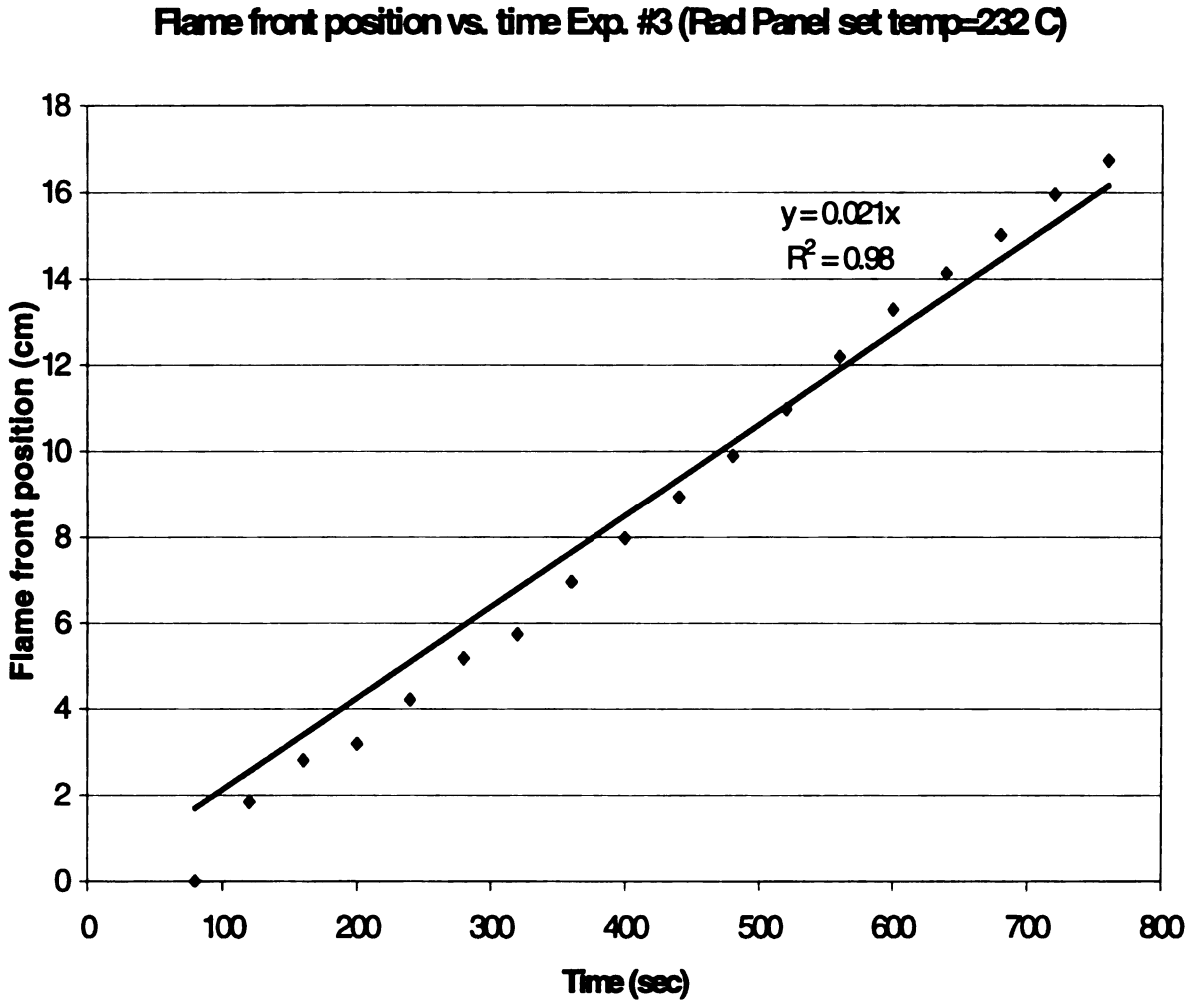

Figure 4.19 Flame front position vs. time for a set radiant panel temperature of 232° C, Experiment # 3.

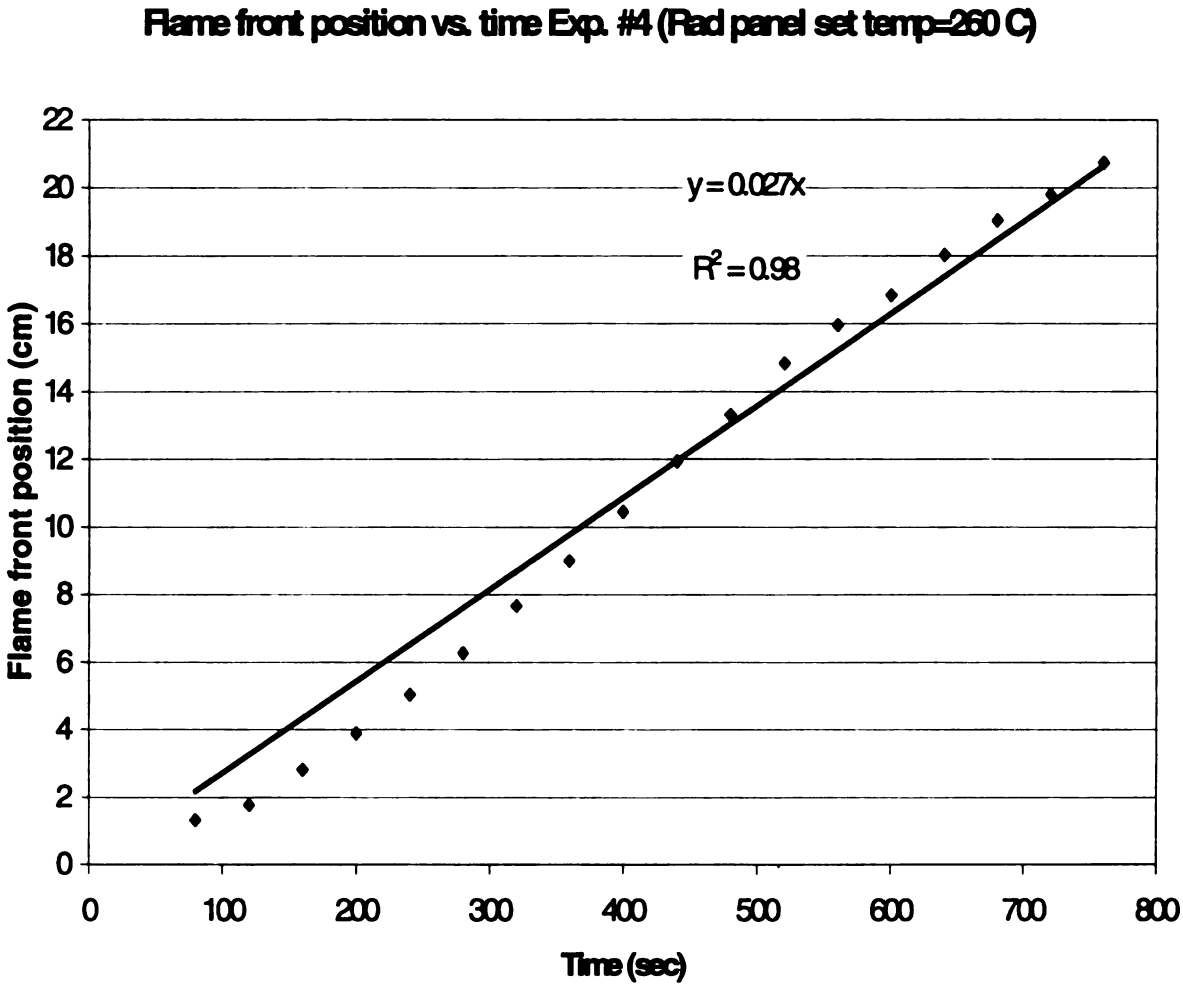

Figure 4.20 Flame front position vs. time for a set radiant panel temperature of 260° C, Experiment #4.

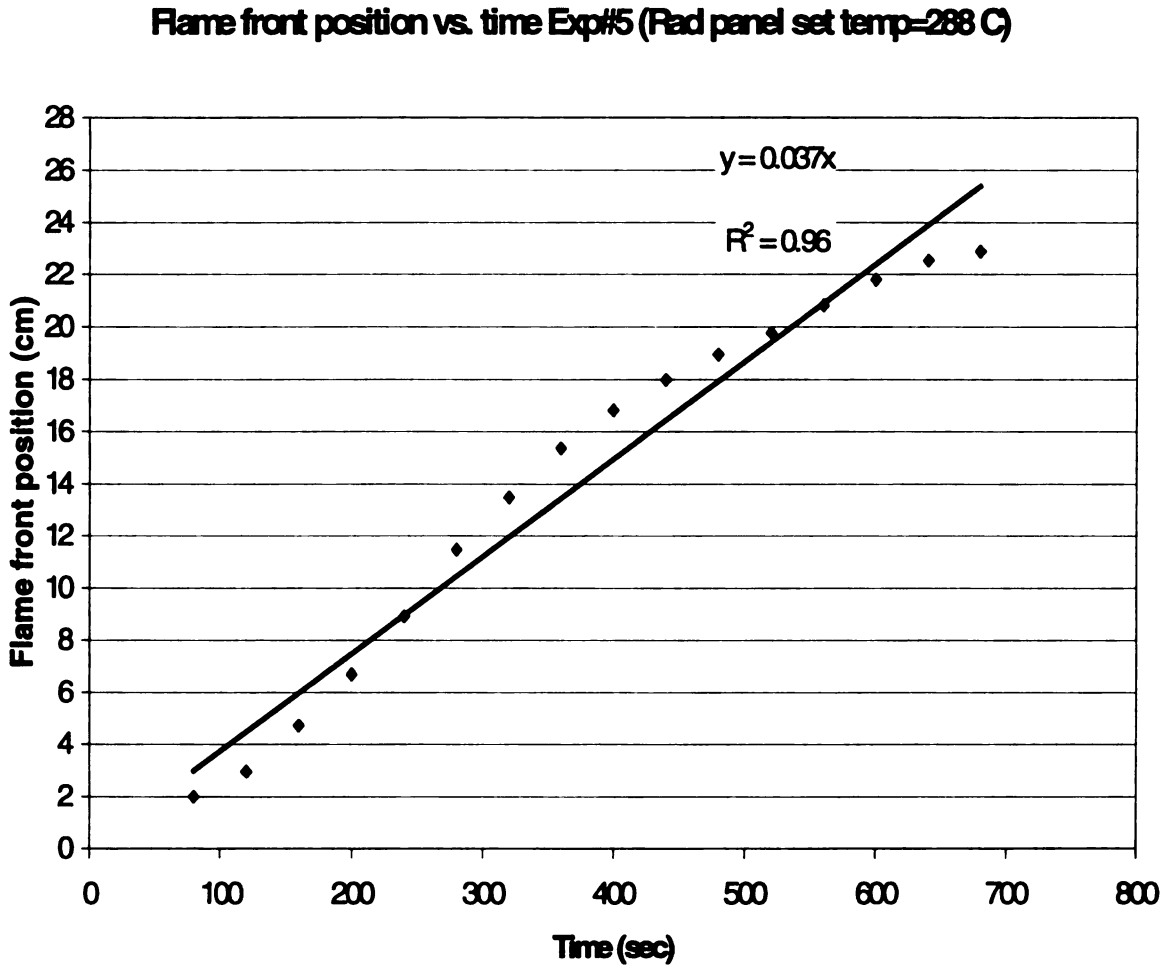

Figure 4.21 Flame front position vs. time for a set radiant panel temperature of 288° C, Experiment #5.

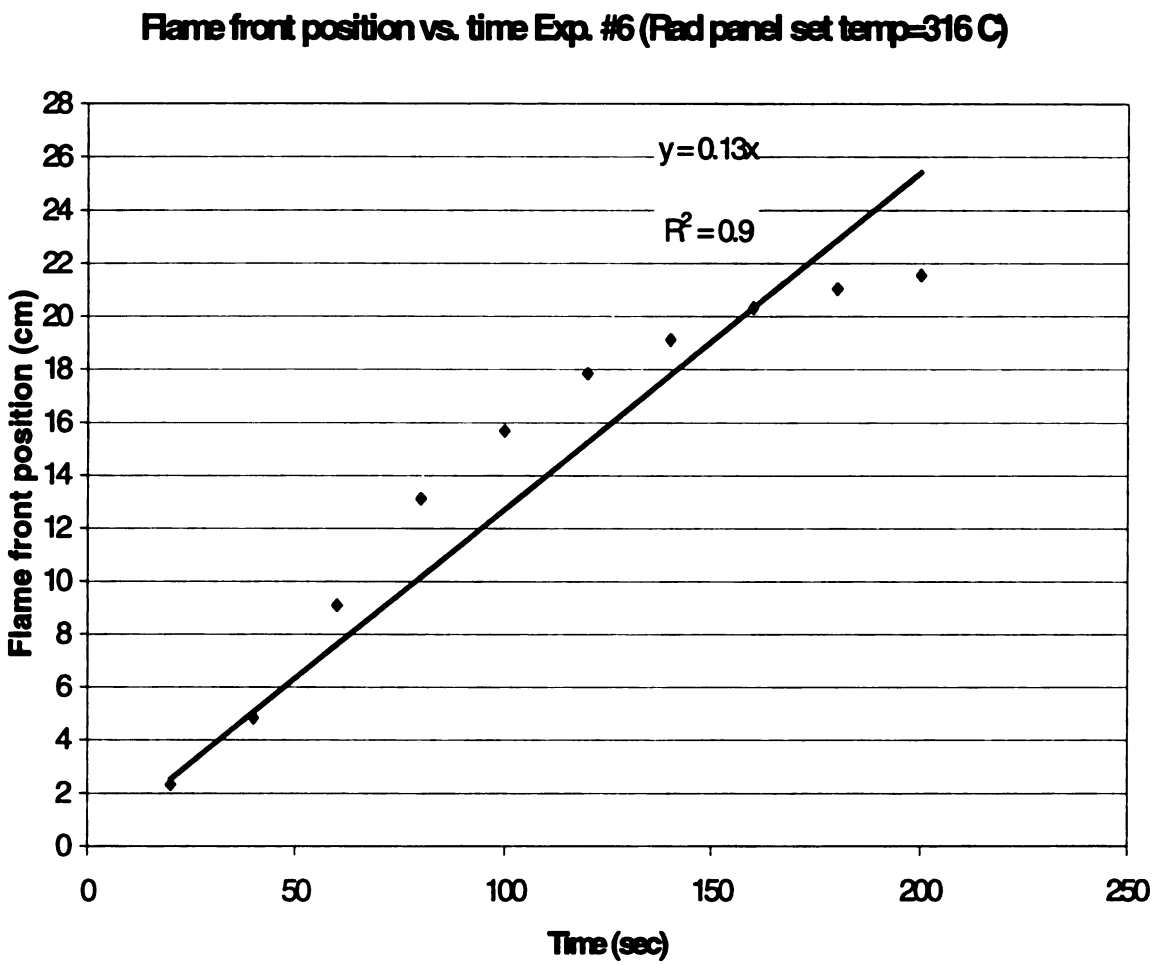

Figure 4.22 Flame front position vs. time for a set radiant panel temperature of 316° C, Experiment #6.

Figure 4.22 (corresponding to experiment #6) indicates a much faster flame spread rate. Because the spread rate was much faster than the previous tests the video capture interval was reduced to 20 seconds. The inflection point has again moved up to around 16cm. As the flame spread rate increases the linearity of the data seems to decrease.

The acceleration in the beginning of the test (near the top of the sample) may be explained by recognizing the fact that the flame front is moving into a region of higher incident heat flux. Four effects possibly cause this higher heat flux near the middle of the test period. The first is the increase in the radiative view factor near the center of the sample, resulting in a higher heat flux. The second is an increased radiant panel temperature near the center compared to the edges (as indicated by the radiant panel thermal images) due to conduction losses near the top. The third explanation for this phenomenon could be that there is an increase in the total sample area that is burning. As more of the sample burns it produces radiation that is absorbed by the unburned fuel sample both directly and from reflection within the combustion chamber. The fourth factor could be a transient issue. The center of the sample has most likely not reached thermal equilibrium as the flame front begins at the top of the sample. As the flame front progresses the sample absorbs more and more heat causing a variation (specifically an acceleration) in the flame-spread rate.

As the flame front moves through this region of high heat flux toward the leading edge of the sample it begins to slow down. This slowdown could be due

to several effects. The first reason for this could be that the heat flux impinging on the unburned surface decreases. This occurs as a result of a decrease in both the radiant panel temperature (due again to conduction losses at the edges) and in the view factor. Additionally, a decrease in temperature at the leading edge of the radiant panel is sure to occur due to forced convection losses, also contributing to a decrease in the heat flux. An additional explanation in the slowdown of the flame spread rate is the thinning of both the hydrodynamic and thermal boundary layers near the leading edge of the sample (in comparison to the trailing edge). This causes an increase in the oxidizer velocity in the near fuel region where combustion is occurring. The increased oxidizer velocity carries away both more gasified fuel and more heat from the sample's surface, which produces a resultant decrease in the flame-spread rate.

As the temperature of the radiant panel increases the effects that contribute to a variation in flame spread rate also increase. This causes a greater deviation from the linear fit resulting in a lowered R^2 value.

Figure 4.23 indicates a much greater increase in the flame-spread rate compared to the previous tests. This test exhibits (while impossible to glean from the figure) the "Oscillatory Flame Advancement (OFA)" behavior discussed in Chapter 5. Because the points are so deviant from any linear curve fit one was not applied and the test was not used in the later comparisons of flame spread rate.

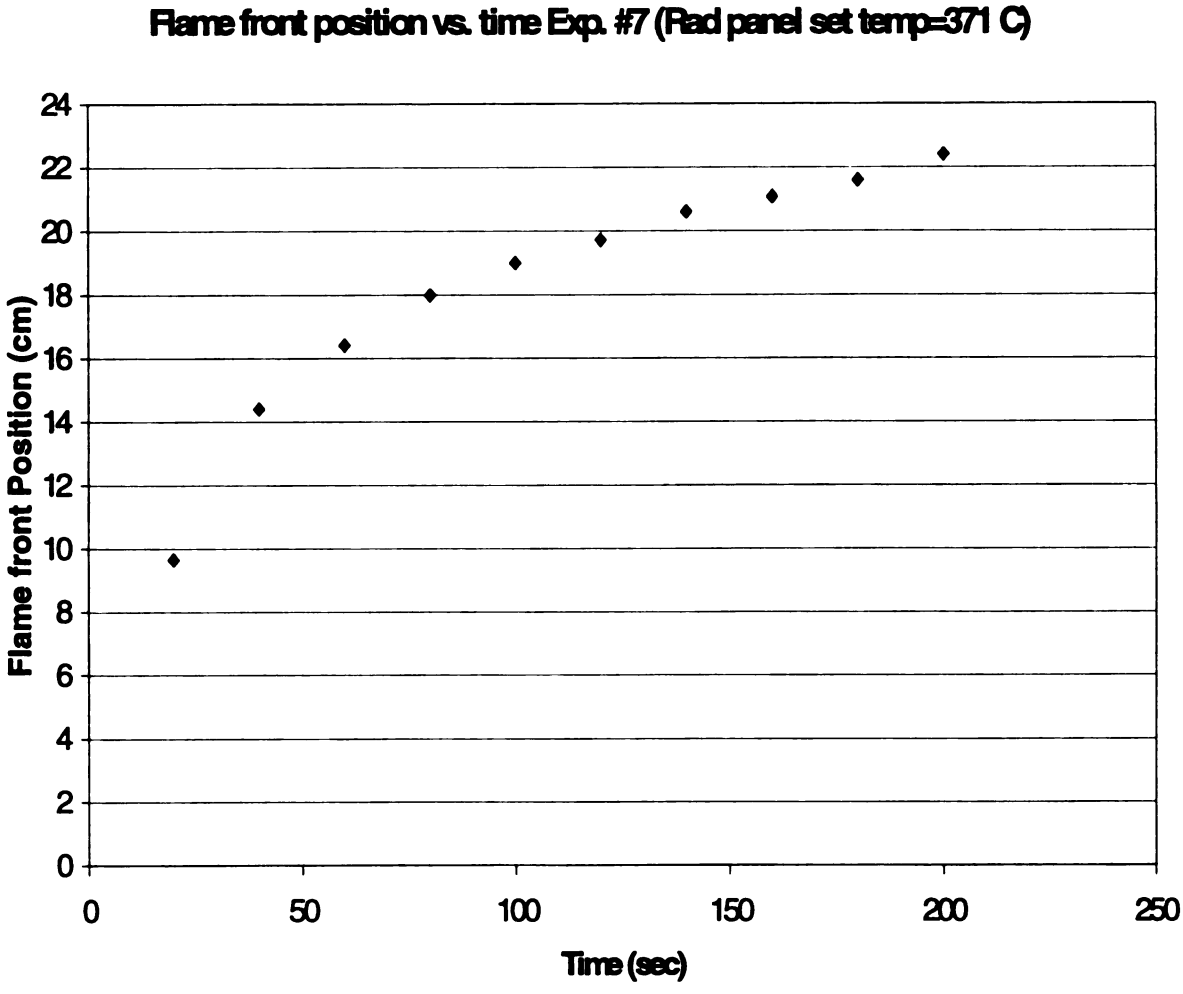

Figure 4.23 Flame front position vs. time for a set radiant panel temperature of 371° C, Experiment #7.

Figure 4.24 represent repeated versions of experiment #4 (radiant panel set temperature of 260° C). It indicates that the repeatability of the experiment is fairly good. The slope of the linear fit variation is small (although the number of tests is not high enough to calculate a reliable standard deviation).

Figure 4.25 represents the linear regression applied to the averaged data at each time level from Figure 4.24. This is the center dotted line shown. The two lines around represent the upper and lower maximum errors associated with estimating the slope and intercept for these data. The error bars are quite close to the central line. This indicates that the variation of the data seen in Figure 4.24 is most likely not due to errors in estimating the slope and intercept of the linear curve fit.

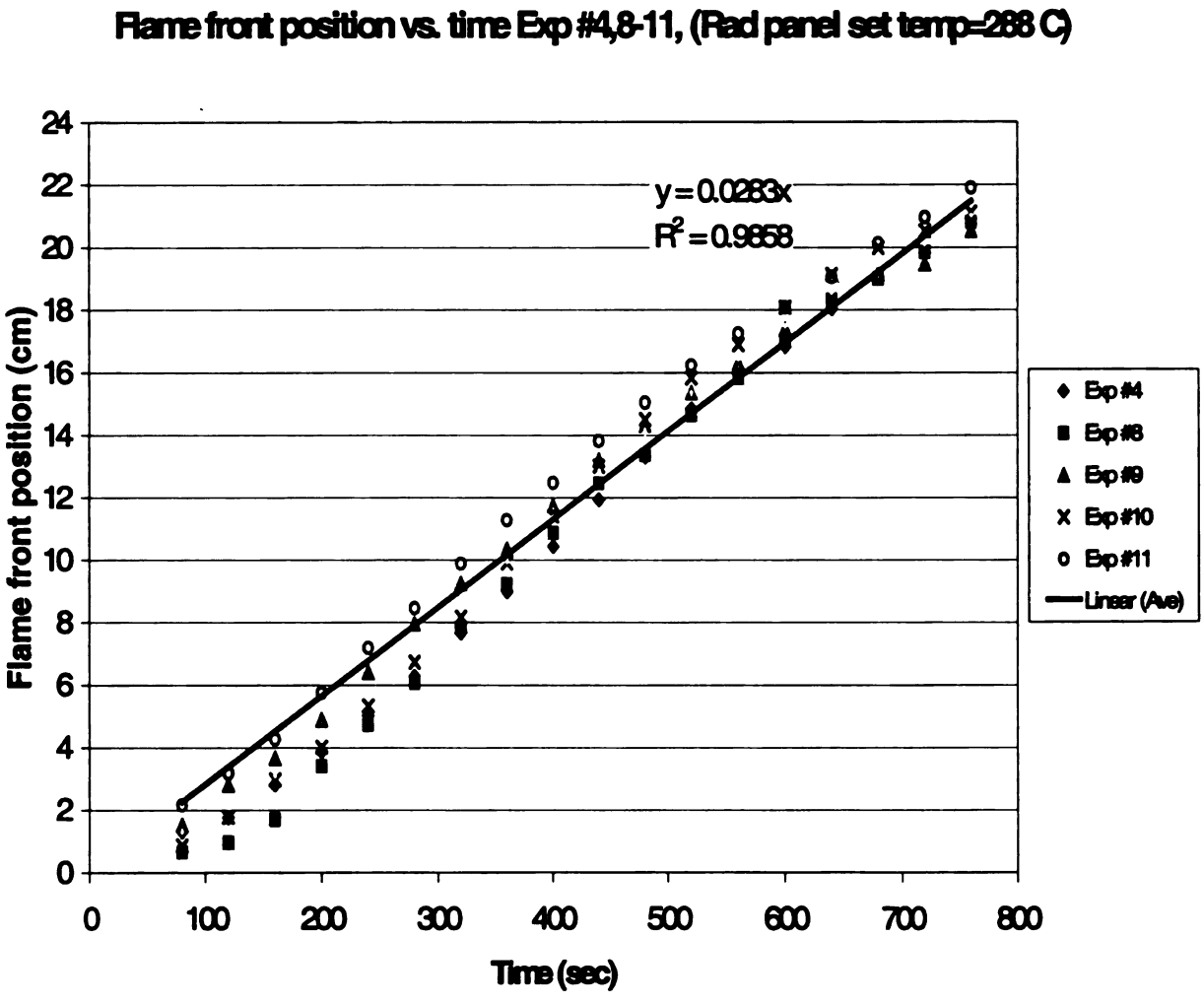

Figure 4.24 Flame front position vs. time for a set radiant panel temperature of 260° C, Experiments #4, 8-11.

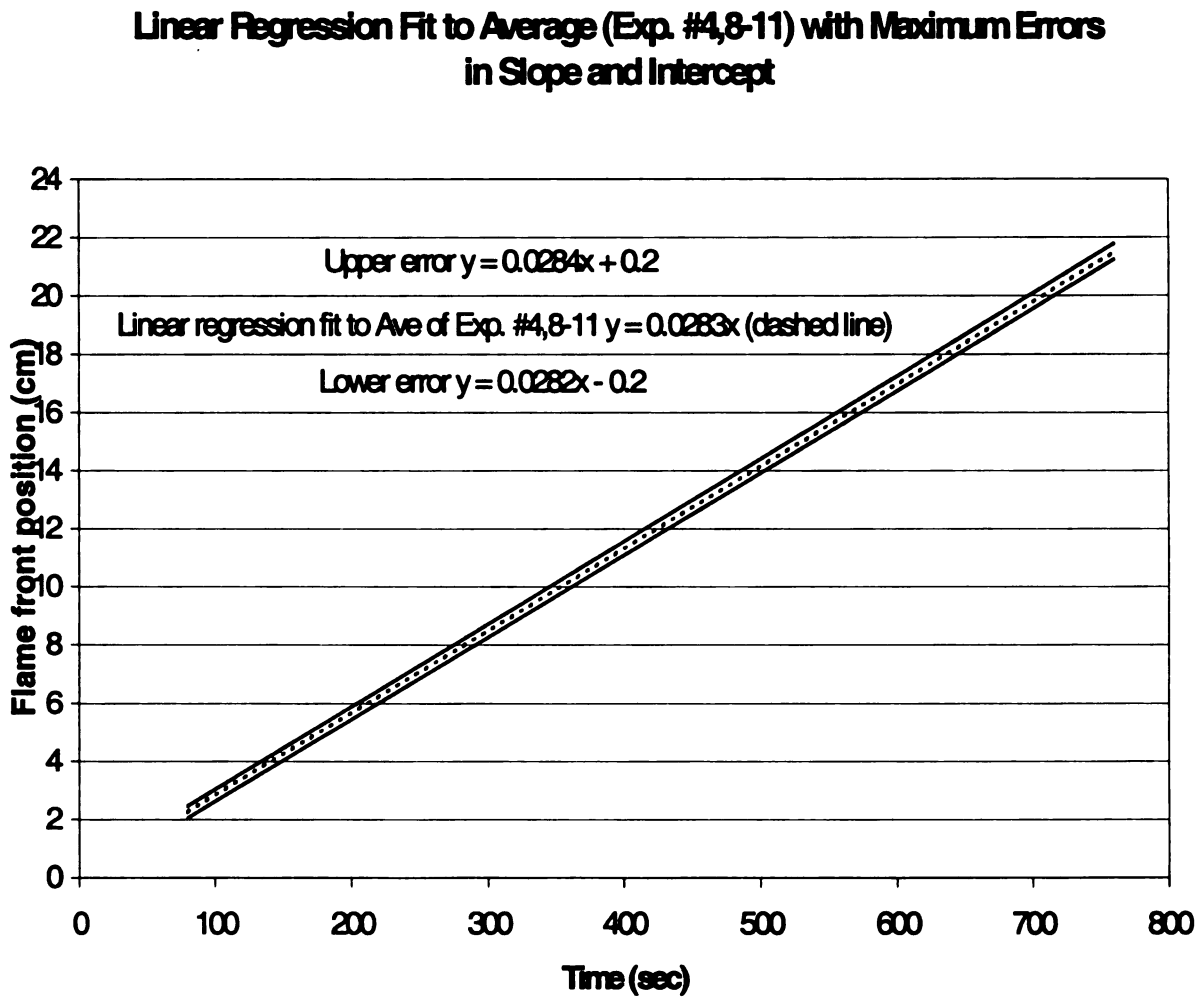

Figure 4.25 Slope of least squares fit for various radiant panel temperature settings, Experiments #1-6, 8-11.

Figure 4.26 is a plot of the slope of the linear curve fits (roughly the average flame spread rate) versus the set radiant panel temperature. This indicates that there is marked increase in the flame-spread rate with the increase in radiant panel temperature. Experiments #1 and #2 may be called into question because they don't necessarily follow the trend. The lack of variation from experiment to experiment is exhibited well by the data taken at the radiant panel set temperature of 260° C.

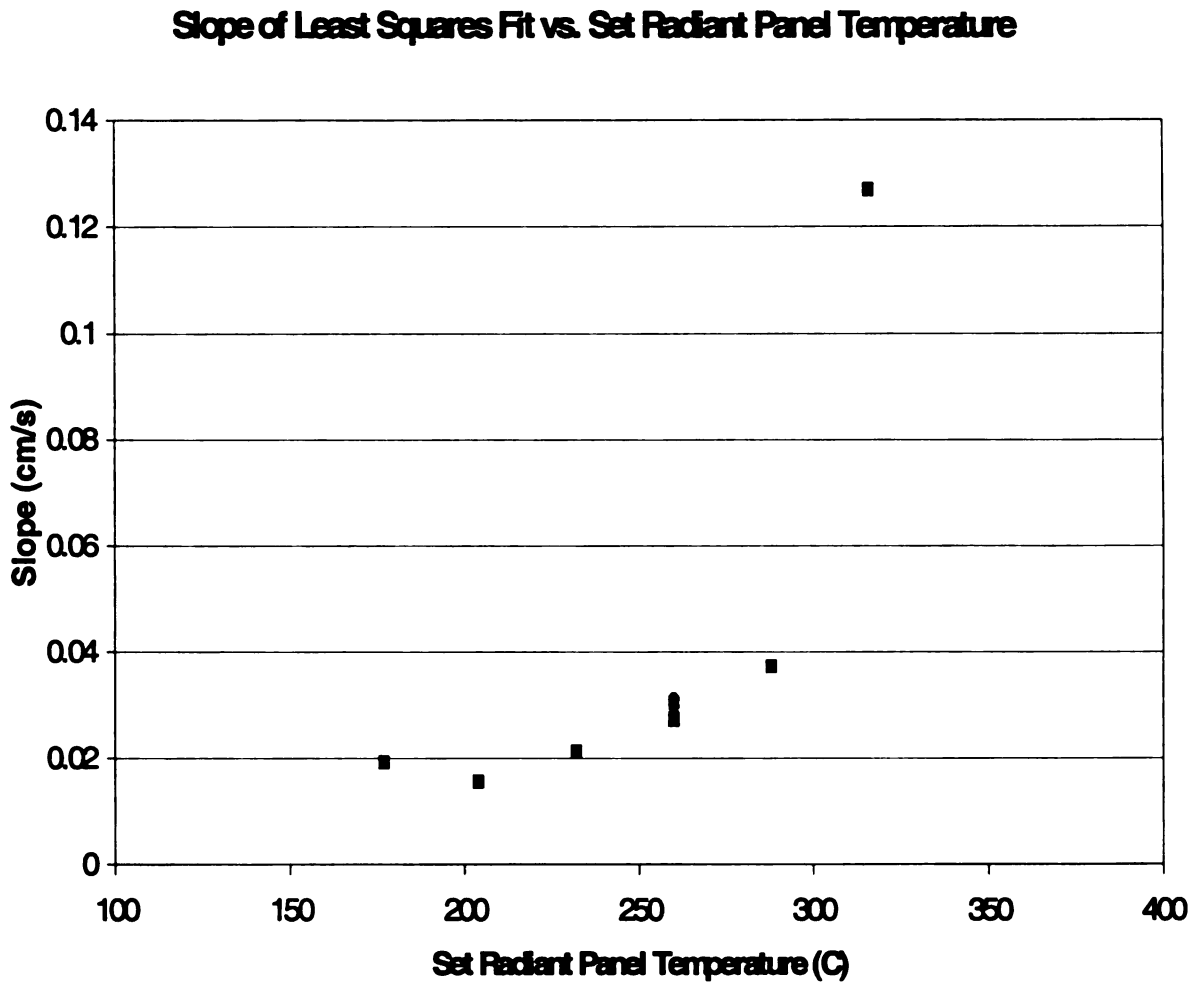

Figure 4.26 Slope of least squares fit for various radiant panel temperature settings, Experiments #1-6, 8-11.

CHAPTER 5

OSCILLATORY FLAME ADVANCEMENT

During the course of testing an interesting phenomenon was discovered. This so-called Oscillatory Flame Advancement (OFA) occurs only under a unique set of operating conditions and was found to involve a large portion of the sample surface area. A conceptual description of this phenomenon and a preliminary theory for its behavior are given.

The area of interest is given in Figure 5.1. For OFA to occur, a portion of the fuel sample's surface must begin to degrade into a highly viscous melt layer. In order to form this melt layer the radiant panel must be heated up to a set temperature above 320° C for a oxidizer flow rate of around 2.25m/s. The panel must be slid into the combustion chamber and a long heat-up period must be given to allow the sample's surface to begin to "boil" or actively degrade. In this state the temperature at which a balance is struck between total heat losses and the heat gained due to the external radiation at the sample surface is higher than the boiling temperature of the fuel. Therefore the sample's surface begins to boil.

After a significant fraction of the surface begins to boil (approximately 2/3 to 3/4 of the surface area) the ignition wire is turned on. A flame front appears near the ignition source and very quickly sweeps over the entire degraded surface. As quickly as it appears it recedes back to the ignition source, completely extinguished over approximately 95% of the sample's surface. This cycle then repeats itself but for this cycle the time interval *between* full

advancement and regression is smaller. With each cycle the process continues and the time interval between advancement and regression is considerably smaller. Additionally, the line to which the flame fully regresses begins to creep down the sample's surface with each successive cycle until the advancement front and regression front meet. Like a rubber ball bouncing between two parallel converging walls that finally leave no room for movement, the flame front oscillations reach a steady state and ultimately a continuous flame engulfs the sample surface.

What causes this unstable behavior? As with other complex transient phenomena it results from a delicate balance between several interrelated competing mechanisms. The rate of fuel evaporation from the liquid state to the gaseous state is related to the temperature of the liquid state. As the temperature of the liquid state increases so does the rate of fuel evaporation to the gaseous state such that $\dot{m}''_{fuel,evp} = f(T_{surface})$

In order for combustion to occur an adequate concentration of fuel (known as the lean limit) must be present in some region Δx (the quenching distance) away from the fuel surface of thickness Δx_f (the flame thickness). In order to produce the lean limit at a distance Δx, therefore, a minimum surface temperature must be achieved. Since the flow field tends to carry away both heat and evaporated fuel, this surface temperature must be higher in the presence of a forced oxidizer flow. Both the external heat flux and the heat flux produced by the flame flash increase this surface temperature. In this way the

heat flux is directly related, through the fuel surface temperature, to the presence of a lean limit.

When the concentration of evaporated fuel reaches the lean limit at a distance Δx and a pilot flame is present at the top edge of the decomposing sample combustion occurs a flame sheet flashes across the surface. The pilot is situated near the trailing edge of the fuel sample where the boundary layer of evaporated fuel is the thickest. The concentration at Δx is above the lean limit and the flame begins to travel down the sample, still in a region where the concentration is above the lean limit. As it travels downward it uses up the fuel in the volume of thickness Δx_f. The temperature at the surface of the fuel is not high enough to produce a fuel evaporation rate that will replace this fuel quick enough. So after the fuel is all burned up within the critical volume the flame extinguishes. The fuel is all burned near the leading edge of the flame front before trailing edge because the thermal, hydrodynamic, and evaporated fuel boundary layers are at their thinnest in this region.

As the flame front burns over the fuel surface (and even after it extinguishes) a heat flux from the flame flash is transferred to the fuel. This heat flux incrementally increases the temperature $(T \rightarrow T + \delta T)$ of the liquid layer and therefore changes the evaporation rate, $\dot{m}'' = \dot{m}(T + \delta T)$. The time required for the concentration of the evaporated fuel to reach the lean limit within the region $\Delta x + \Delta x_f$ now becomes smaller. In other words as the evaporation rate increases the time delay between successive flame front advancements decreases (Fig. 5.2).

This effect creates an acceleration in the oscillatory cycle until a steady state is reached. The evaporation rate has increased to such a degree by the time steady state is reached that it is now delivering an ample amount of fuel to the burning region even to the point of causing fuel rich combustion (noted by its yellowish-orange appearance and soot laden products of combustion).

The change in surface temperature necessary to produce the large increase in fuel evaporation seen, however, is most likely not caused by the external heat flux. Since the time required for this whole process (from first flash to continuous flame) to occur is between 10 and 15 seconds the heat flux from the flame front seems to be the more likely candidate. Because the heat flux from the flame is most likely the driving mechanism behind the acceleration in the oscillations perhaps these two parameters could be linked. This may enable measurements of the oscillation frequency to be used as a rough predictor of the heat flux from the flame to the fuel surface (a rather elusive quantity).

The creation of a rigorous theoretical model of OFA could prove difficult due to the complexity of the system. An easier (and perhaps more fruitful) path would make used of some simplifications in the governing physical system. One such simplification would eliminate the reaction equations by simply replacing the combustion with a transient volumetric heat generation term, inserted into the energy equation, but it is not yet clear how accurate such a model might be. The development of such a model is beyond the scope of this thesis.

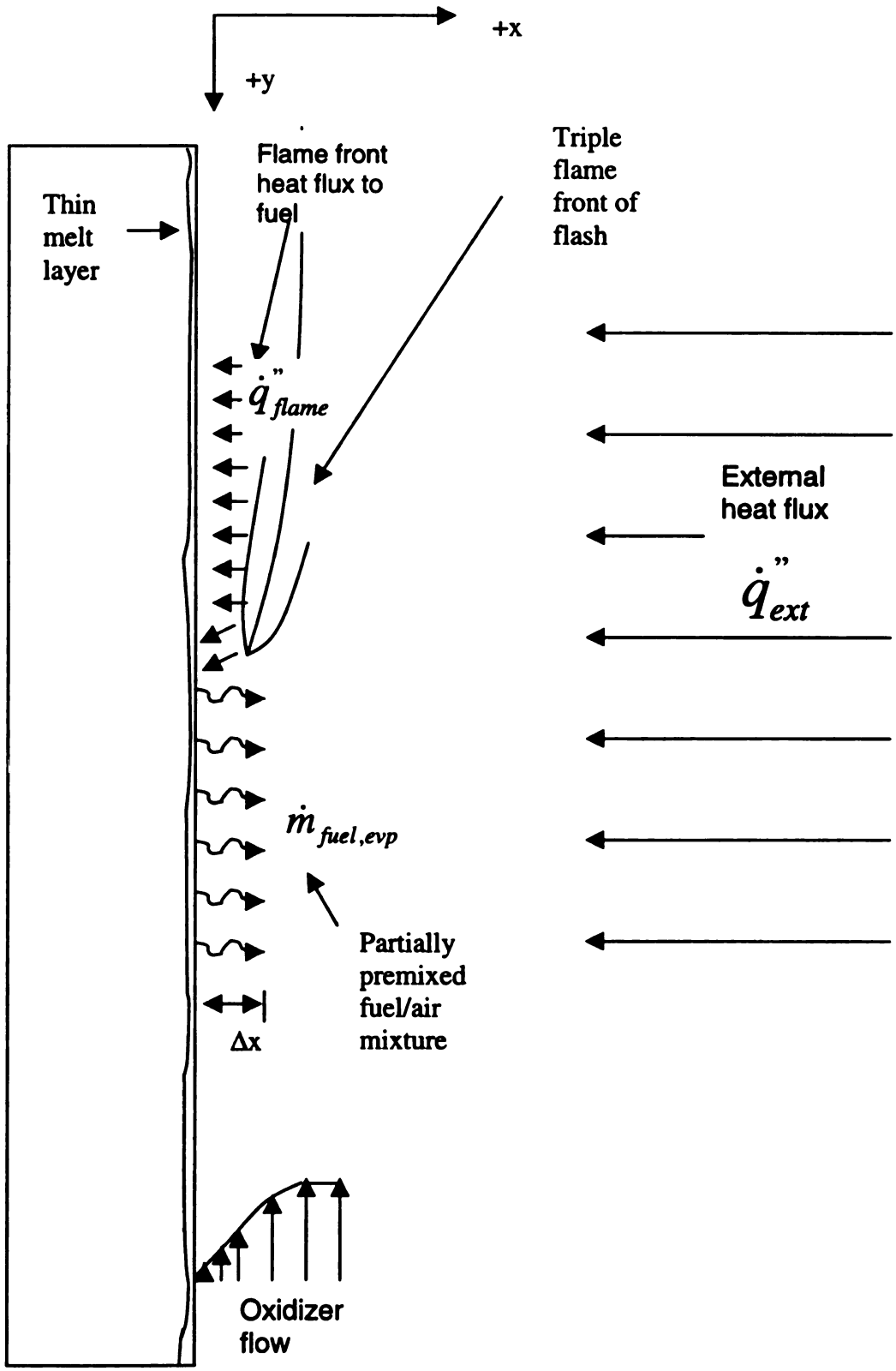

Figure 5.1 The region under consideration for the OFA phenomenon.

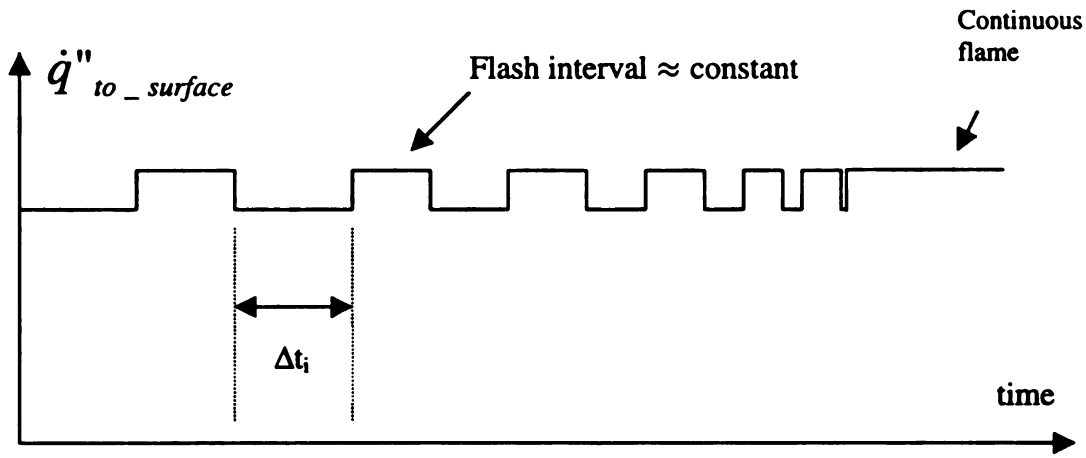

$t_I \rightarrow 0$ as $t \rightarrow \infty$

Figure 5.2 The heat flux to the surface as a function of time for the OFA theory.

CHAPTER 6

CONCLUSIONS AND RECOMMENDATIONS FOR FUTURE WORK

Preliminary testing of the MSU Fire Tunnel and its components indicate that nearly all of the original design goals have been met. The flow field within the chamber is predictable, the radiant panel is effective, and the flame-spread tests were successful and appear highly repeatable.

It has been shown that the flow field within the combustion chamber is largely laminar and predictable. The hydrodynamic boundary layer near the fuel sample surface has been shown to be thin and nearly unaffected by the rest of the combustion chamber surfaces.

The radiant panel has proven to be a durable radiant energy source that is easy to regulate, control and use. While there seems to be some non-uniformities across its surface they are not large and with a little effort could be easily corrected.

Flame-spread tests indicate that the MSU Fire Tunnel is capable of producing the predictable, repeatable environmental conditions necessary for precise solid fuel ignition and flame spread studies. While the tests need to be refined the initial results look promising and indicate that this device could contribute a great deal to the knowledge of solid fuel combustion.

The MSU Fire Tunnel is a versatile device. It can perform combustion as well as basic heat transfer experiments. For example, temperature profiles along the surface of the sample have been generated for use in other studies using a

data acquisition unit and a series of thermocouples. The oxygen concentration of the oxidizer flow, the flow velocity, the level of radiant flux, the type of sample tested, the location of the ignition source, as well as other parameters can all be varied.

While the MSU Fire Tunnel has exhibited promising preliminary results, several improvements could be made to increase its effectiveness. The major areas were improvements need to be made are in the flow system, the radiant panel, and the sample holder. While not really in the scope of this project the method of acquiring data could also be improved quite easily.

A few improvements in the flow system would improve the precision and operating range of the device. The blower is a bit undersized and a more powerful blower would allow for a greater range of flow velocities to be studied. It may even allow for the study of a forced turbulent flow field, an interesting problem. Also, examining the flow profiles with radiant heating (and possibly even a burning sample) would prove very useful. Particle seeding techniques would most likely be necessary to obtain this data. These techniques, while expensive and somewhat complicated, enable measurements to be obtained under high temperature conditions.

The uniformity of the radiant panel could be improved by using an additional set of radiant strip heaters. In order to compensate for the lack of a uniform heat flux (lower levels near the edges) due to the view factor and conduction losses the temperature of the edge of the panel could be raised using another set of strip heaters. The heaters could be placed on the back of the

existing heaters and bound with a highly conductive paste thus creating a temperature bulge near the edges of the radiant panel. This bulge could be fine tuned using the thermal imaging system and theoretical calculations in order to compensate for the view factor difference. This may allow a uniform flux to be produced from the perspective of the fuel sample. Making the heat flux more uniform will most likely correct the u-shaped non-uniformity present in nearly all of the tested samples.

Also, isolation of the various effects that may cause the velocity variation in the flame spread (as indicated by the inflection point on the flame-spread rate curve) would allow for a greater knowledge of the relative intensities of these effects. The radiant panel could be moved with respect to the fuel sample to determine the relative effect of the radiant panel view factor. The fuel sample could be moved with respect to the elliptical shape to determine the relative effect of the thinning boundary layers.

Further investigation into the near-fuel boundary layer is necessary. Investigation into the validity of the flat plate assumption would be useful. In order to determine if there is no pressure gradient in the free stream (implicit in the flat plate assumption) velocity measurements could be made at various streamwise locations. Additionally, the stability of the boundary layer could be investigated by performing more hot wire tests.

Improvements in the sample holder may correct the smaller wave-like non-uniformities along the flame front. As the flame-spread tests progressed the dry wall filler used to smooth the transition between the Marinite sample holder

and the leading edge of the fuel sample began to break down. This may cause some unpredictable fluid flow over the sample surface. Better, high temperature filler could be used to correct this.

Better measurement techniques would certainly improve the resolution of the data. Instead of simply measuring the furthest point of flame spread it may be possible to characterize an average flame front location as well as characterize the degree of non-uniformity along the flame front using image processing tools and some simple mathematical models. Measurements of the fuel surface (as well as within the surface) could easily be performed using thermocouples and the existing data acquisition unit.

The addition of the fin on the trailing edge of the sample holder would improve the uniformity of the flow profile within the combustion chamber. Several designs were tested and they failed for a number of reasons. Because the flames impinge on the surface of the fin it gets very hot. This causes the fin to expand and warp, causing sealing problems. If the seal between the trailing edge of the sample holder and the leading edge of the fin is not perfect, the fire tends to go through it causing the fin to warp even more. One possible solution would be to avoid using the fin altogether and introduce a separate blower. This blower could be arranged so that it sucked air out of the combustion chamber behind the end of the sample holder. Several hoses could be used so as to avoid point source suction that may compromise spanwise uniformity.

Further investigation into the Oscillatory Flame Advancement phenomenon could lend additional insight into nature of flame spread over solid

fuels. The frequency of the oscillations in the experimental device could be obtained by simply monitoring the audio signal generated. As the flame advances over the fuel surface it creates a noticeable sound. This sound corresponds with the frequency of the advancement. The intensity of the audio signal could be monitored and the locations of the peaks in the intensity may correlate with the frequency of the oscillations.

If the analytical model of OFA could be advanced further, a hybrid analytical/experimental analysis may allow for the calculation of the heat flux from the flame to the sample surface for a given set of operating conditions. Because the heat flux is the driving mechanism in this phenomenon, it may be possible to relate it to the acceleration in the advancement frequency. Once the advancement frequency is known it might be able to be plugged into an analytical model to determine what heat flux is necessary to produce this frequency for a given set of conditions. The analytical model for this phenomenon is in the initial stages of development.

APPENDIX

Operating Instructions for The MSU Fire Tunnel

1.1 Introduction

These instructions are designed to allow a user to operate the MSU Fire Tunnel who has no previous experience with it. It is assumed at the beginning of the instruction that the MSU Fire Tunnel is in a storage configuration. The MSU Fire Tunnel is in the storage configuration when the sample holder is out of the combustion chamber, the radiant panel is mounted onto the hood, and (obviously) all power is off and all of the components are unplugged.

1.2 Performing Flame-Spread Tests with the MSU Fire Tunnel

A fuel sample must be mounted into the sample holder. The back of the sample holder has nine holes for mounting screws. Pre-drill holes (appropriate for the mounting screws) approximately 1/4" into the fuel sample. Once the fuel sample is secured into place the edges should be filled. This can be done with interior spackling paste but it is not ideal. A filling compound that does not crack and expand when heated would be better. Fiberglass insulation can be used to fill the gaps that are not as critical to the flow over the sample holder.

The back of the sample holder has four spacers and bolts. The bolts can be inserted into the holes on the combustion chamber and secured with washers and nuts.

The radiant panel can now be mounted to the combustion chamber. The (safety) bolts used to mount the radiant panel to the hood are also used to prevent the panel from sliding out of position. Remove the radiant panel from its

position on the hood and slid it partially into the slots cut into the combustion chamber. Now remove the safety bolts and slide the panel in. Replace the safety bolts and secure with nuts.

Important! Check each terminal connecting the radiant panel to the high-temperature lead wires. The wires leading to the terminals become loose with time and must be replaced periodically.

The ignition wire system can now be installed. Insert the hollow ceramic tubes from the outside of the combustion chamber. Next, insert the igniter assembly into the ceramic tubes. The steel wires of the ignition assembly should stick out of the ceramic tubes about 1/4 inch. The leads from the variable voltage supply can now be attached to the ignition wire. Electrical tape (while not ideal) works well.

The components can now begin to be plugged in and turned on. Plug in and turn on the blower (Fig. A.1), the pressure transducer power supply, and the voltmeter. Adjust the damper on the blower to the desired flow-rate (referring to the pressure transducer output).

Mount the camera or other measuring equipment.

Be sure that the butterfly valve at the top of the hood is open. Turn on the hood and shut the glass slide.

Slide out the radiant panel.

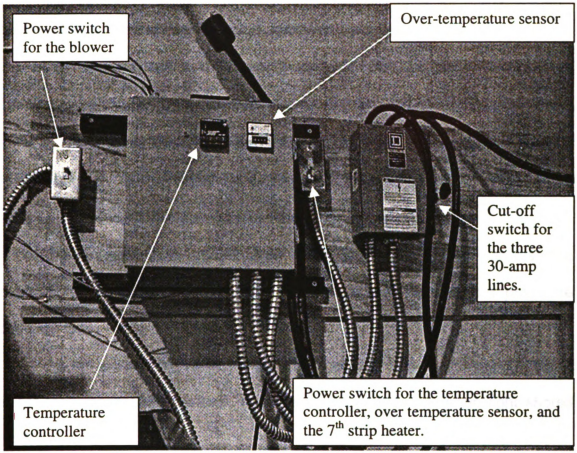

Figure A.1 The radiant panel control system, component switches, and supporting equipment.

Plug in the variable voltage supply and the power supply for the temperature controller. Turn on the power to the temperature controller.

Note: The top strip heater is powered from the same circuit that powers the temperature controllers. When the controller is on that line is live! The SSRs are off when there is no control voltage. If the set temperature on the temperature controller is lower than the room temperature the SSR should not trip. However,

don't maintenance the radiant panel if any power is on to the control system. Ground potential, thermocouple noise, ect. could cause the SSR to trip even if the set temp is less than the room temperature.

Turn on the power to the power to the controller. Set the desired radiant panel temperature (°F) by holding down the * and simultaneously pressing the ↑ or the ↓. Flip the big disconnect switch into the on position. The radiant panel is now heating up. The controller will display the measured temperature. For more detail on the temperature controller see the CN9120A manual.

The temperature is measured on the bottom of the radiant panel so the response is slow. The controller could be re-tuned (see manual) to improve the response time.

Set the desired high-limit temperature. Usually it is set to around 100° F higher than the set temperature. Push the reset button. A green light should appear.

Important: If this light goes off it means that he temperature has exceeded the set temperature and the system should be shut down immediately.

Slide the radiant panel into the combustion chamber once it has reached the desired temperature. Usually a sample heat-up time period is waited before the ignition wire is turned on. Turn on the ignition wire by dialing in a voltage on the variable voltage power supply. A calculation can be made to determine the voltage necessary to run the desired current through the wire. Tables on the relationship between the current through the wire and the temperature of the wire can be found in the Omega Temperature catalog. Usually the wire is heated until

glows a bright orange. Care must be taken so that the wire is not heated too much and broken.

After the fuel sample is lit the ignition wire must be turned off in order to prevent it from breaking.

Turn off the radiant panel when the test is complete.

In order to extinguish the fire an injection of nitrogen is used. Open the main valve for the bottled nitrogen cylinder and open the pressure regulator valve. Turn off the blower. The fire should be extinguished in about ten to twenty seconds.

Turn off and unplug all equipment.

BIBLIOGRAPHY

BIBLIOGRAPHY

(1) Wichman, I.S., "A Review of the Literature of Material Flammability, Combustion, and Toxicity Related to Transportation", unpublished.

(2) ASTM E 84 – 97a, "Standard Test Method for Surface Burning Characteristics of Building Materials", *Annual Book of ASTM Standards*, Vol. 4.07, 1997.

(3) ASTM E 1354 – 97, "Standard Test Method for Heat and Visible Smoke Release Rates for Materials and Products Using an Oxygen Consumption Calorimeter", *Annual Book of ASTM Standards*, Vol. 4.07, 1997.

(4) ASTM E 1740 – 97a, "Standard Test Method for Determining the Heat Release Rate and Other Fire-Test-Response Characteristics of Wallcovering Composites Using a Cone Calorimeter", *Annual Book of ASTM Standards*, Vol. 4.07, 1997.

(5) ASTM E 648-97, "Standard Test Method for Critical Radiant Flux of Floor-Covering Systems Using a Radiant Heat Energy Source", *Annual Book of ASTM Standards*, Vol. 4.07, 1997.

(6) ASTM E 1321 – 97a, "Standard Test Method for Determining Material Ignition and Flame Spread Properties", *Annual Book of ASTM Standards*, Vol. 4.07, 1997.

(7) J.L. Cordova, J. Ceamanos and A.C. Fernandez-Pello, "Piloted Ignition of a Radiatively Heated Solid Combustible Material in a Forced Oxidizer Flow", 7th AIAA/ASME Joint Thermophysics and Heat Transfer Conference, June 15-18 1998.

(8) J. Quintiere, M. Harkleroad and D. Walton, "Measurement of Material Flame Spread Properties," *Combustion Science and Technology,* 1983, Vol32, pp. 67-89.

(9) J.G. Quintiere, *Principals of Fire Behavior,* Delmar Publishers, 1998, p. 98

(10) J.L. Cordova, J. Ceamanos and A.C. Fernandez-Pello and R.T. Long, J.L. Torero, J.G. Quintiere, "Flow Effects on the Flammability Diagrams of Solid Fuels", Paper Proceedings of the 1997 4th International Microgravity Combustion Workshop, 1997.

(11) T., Morel, "Design of Two-Dimensional Wind Tunnel Contractions", *Journal of Fluids Engineering, Trans. ASME,* Vol. 99, 1977, pp. 371-378.

(12) Foss, J., Personal communication.

(13) Design Procedure For Optimum 2-D Wind Tunnel Contraction, B. Voss, 1990, Dos based computer program.

(14) Schlichting, H., Boundary Layer Theory, Pergamon Press, New York (1955).

(15) R. Siegel, J.R. Howell, *Thermal Radiation Heat Transfer,* Hemisphere Publishing Corp., 2nd Edition, 1981.

(16) I. Miller, J.E. Freund, *Probability and Statistics for Engineers*, Prentince-Hall, Inc. 1965.

MICHIGAN STATE UNIV. LIBRARIES
31293021061811